MATERIALS SCIENCE

Guokui Liu
Bernard Jacquier (Eds.)

Spectroscopic Properties of Rare Earths in Optical Materials

Springer Series in
MATERIALS SCIENCE 83

Springer Series in

MATERIALS SCIENCE

Editors: R. Hull R. M. Osgood, Jr. J. Parisi H. Warlimont

The Springer Series in Materials Science covers the complete spectrum of materials physics, including fundamental principles, physical properties, materials theory and design. Recognizing the increasing importance of materials science in future device technologies, the book titles in this series reflect the state-of-the-art in understanding and controlling the structure and properties of all important classes of materials.

62 **Epitaxy**
Physical Principles
and Technical Implementation
By M.A. Herman, W. Richter, and H. Sitter

63 **Fundamentals**
of Ion-Irradiated Polymers
By D. Fink

64 **Morphology Control of Materials**
and Nanoparticles
Advanced Materials Processing
and Characterization
Editors: Y. Waseda and A. Muramatsu

65 **Transport Processes**
in Ion-Irradiated Polymers
By D. Fink

66 **Multiphased Ceramic Materials**
Processing and Potential
Editors: W.-H. Tuan and J.-K. Guo

67 **Nondestructive**
Materials Characterization
With Applications to Aerospace Materials
Editors: N.G.H. Meyendorf, P.B. Nagy,
and S.I. Rokhlin

68 **Diffraction Analysis**
of the Microstructure of Materials
Editors: E.J. Mittemeijer and P. Scardi

69 **Chemical-Mechanical Planarization**
of Semiconductor Materials
Editor: M.R. Oliver

70 **Applications of the Isotopic Effect**
in Solids
By V.G. Plekhanov

71 **Dissipative Phenomena**
in Condensed Matter
Some Applications
By S. Dattagupta and S. Puri

72 **Predictive Simulation**
of Semiconductor Processing
Status and Challenges
Editors: J. Dabrowski and E.R. Weber

73 **SiC Power Materials**
Devices and Applications
Editor: Z.C. Feng

74 **Plastic Deformation**
in Nanocrystalline Materials
By M.Yu. Gutkin and I.A. Ovid'ko

75 **Wafer Bonding**
Applications and Technology
Editors: M. Alexe and U. Gösele

76 **Spirally Anisotropic Composites**
By G.E. Freger, V.N. Kestelman,
and D.G. Freger

77 **Impurities Confined**
in Quantum Structures
By P.O. Holtz and Q.X. Zhao

78 **Macromolecular Nanostructured**
Materials
Editors: N. Ueyama and A. Harada

79 **Magnetism and Structure**
in Functional Materials
Editors: A. Planes, L. Manõsa,
and A. Saxena

80 **Ion Implantation**
and Synthesis of Materials
By M. Nastasi and J.W. Mayer

81 **Metallopolymer Nanocomposites**
By A.D. Pomogailo and V.N. Kestelman

82 **Plastics for Corrosion Inhibition**
By V.A. Goldade, L.S. Pinchuk,
A.V. Makarevich and V.N. Kestelman

83 **Spectroscopic Properties of Rare Earths**
in Optical Materials
Editors: G. Liu and B. Jacquier

Volumes 10–61 are listed at the end of the book.

Guokui Liu Bernard Jacquier (Eds.)

Spectroscopic Properties of Rare Earths in Optical Materials

With 194 Figures and 61 Tables

Springer

Dr. Guokui Liu
Chemistry Division
Argonne National Laboratory
Argonne, IL 60439
USA
E-mail: gkliu@anl.gov

Professor Bernard Jacquier
Université Lyon1, CNRS
10 rue André Marie Ampère
69622 Villeurbanne
France
E-mail: jacquier@pcml.univ-lyon1.fr

Series Editors:

Professor Robert Hull
University of Virginia
Dept. of Materials Science and Engineering
Thornton Hall
Charlottesville, VA 22903-2442, USA

Professor Jürgen Parisi
Universität Oldenburg, Fachbereich Physik
Abt. Energie- und Halbleiterforschung
Carl-von-Ossietzky-Straße 9–11
26129 Oldenburg, Germany

Professor R. M. Osgood, Jr.
Microelectronics Science Laboratory
Department of Electrical Engineering
Columbia University
Seeley W. Mudd Building
New York, NY 10027, USA

Professor Hans Warlimont
Institut für Festkörper-
und Werkstofforschung,
Helmholtzstraße 20
01069 Dresden, Germany

ISSN 0933-033X

ISBN 3-540-23886-7 Springer Berlin Heidelberg New York

ISBN 7-302-07409-7 Tsinghua University Press

Library of Congress Control Number: 2004114853

Cover concept: eStudio Calamar Steinen
Cover production: *design & production* GmbH, Heidelberg

Printed on acid-free paper SPIN: 10926611 57/3141/di 5 4 3 2 1 0

《Spectroscopic Properties of Rare Earths in Optical Materials》

Preface

Decades of scientific research on spectroscopic properties of f-shell electrons has spawned an extensive array of applications for rare-earth activated luminescent and laser materials. From phosphors activated by Eu^{2+}, Eu^{3+} and Tb^{3+} ions for lighting and display to crystals and glasses doped with Er^{3+} and Yb^{3+} for infrared-to-visible up-conversion, rare-earths represent a large share of the lighting materials market. Currently, Nd^{3+} doped crystals such as Nd^{3+}: YAG ($Y_3Al_5O_{12}$) and Nd^{3+}: YVO_4 are the dominant laser media for high power and compact solid-state lasers, while Er^{3+} doped phosphate and silicate glasses prevalent in optical fiber amplifiers and microlasers used in optical telecommunications. Thanks also to materials science development, rare-earths will receive even wider use in the future, entering in the new world of nanotechnologies for instance. In addition to rare-earth activated phosphors and solid-state lasers, optical applications of rare-earths are already an integral part of internet and data communications and are expected to be applied to information storage and processing, and organic and biological devices.

Since the 1960s, several classic books on spectroscopy of rare-earth ions in solids have been published, including those by Wybourne (1965) and Hüfner (1978). More recent advances in spectroscopic theory and laser experiments involving rare-earth ions in solids were also reviewed, for example, in the book edited by Kaplyanskii and Macfarlane (1987). However, in the f-elements research community, we feel the need of a book that updates the information of recent progresses in the field and facilitates understanding and applications of the principles and concepts that are required in rare-earth optical materials characterization and development. The goal of this book is to provide a connection between basic research and materials science through analysis of fundamental spectroscopic properties of rare-earth activated luminescent and laser optical materials. In addition, this book will serve as an updated reference for materials research by covering a number of currently active topics in the field of rare-earth photo-physics and photo-chemistry. Fundamental topics of optical

spectroscopy are addressed with an emphasis on the physical interactions that determine the primary optical properties, including energy level schemes, transitions intensities, line broadening, mechanisms of non-radiative relaxation and energy transfer. Topics of applied research are selected from recent advances in concepts and techniques that created significant opportunities for present and future applications of rare-earth optical materials.

An international collaboration, which includes contributions from authors with both experimental and theoretical expertise, enables us to offer the reader a systematic review of fundamental aspects and to provide a wide coverage on new applications that utilize the electronic transitions of rare-earth ions in solid-state materials. From free-ion and crystal-field energy level structures to transition intensities and line broadening induced by ion-ion and ion-phonon interactions, the first four chapters survey the fundamentals of f-element photo-physics and spectroscopy, and provide a theoretical framework for the subjects that are discussed in the rest of the book. From Chapter 5 onwards, each chapter is devoted to a particular area of importance in new materials characterization or technology development. From up-conversion phenomena, to materials requirements for frequency-domain and time-domain optical memory, to current progress in rare-earth laser materials and phosphors, the concepts and principles discussed in this book were taken directly from the forefront of research in rare-earth optical materials. Moreover, illustration of current progress in fundamental aspects of quantum confinement and quantum electrodynamics is also discussed. To make it easier to read, and also to avoid cluttering up Chapters 1, 2 and 3, the more theoretical derivations of these chapters are given in Appendices A and B. We hope that this book will provide useful information to researchers and students in the field of f-element spectroscopy and materials development.

Although chapters in this book are written independently by individual authors, significant efforts have been made to achieve a coherent connection and systematic balance for the book as a whole. We are grateful to all authors of this book for their excellent contributions.

Guokui Liu
Argonne, Illinois, USA

B. Jacquier
Lyon, France

Contents

List of Contributors

Editors:

Guokui Liu — Chemistry Division, Argonne National Laboratory, Argonne, Illinois 60439, USA
Tel. 630 262 4630, Fax 630 252 4225
E-mail: gkliu@anl.gov

B. Jacquier — Universite Claude Bernard Lyon 1, 43 bd du 11 Novembre 1918, Villeurbanne F-69622, France
Tel. 33-(0)4 72 44 83 36, Fax 33-(0)4 72 43 11 30
E-mail: Jacquier@pcml.univ-lyon1.fr

Chapter Authors:

Guokui Liu (Chapter 1)

M. F. Reid (Chapter 2) — Department of Physics & Astronomy, University of Cantebury, Christchurch 8020, New Zealand
Tel. 64 3 364 2548, Fax 64 3 364 2469
E-mail: m.reid@phys.canterbury.ac.nz

B. Z. Malkin (Chapter 3) — Physics Department, Kazan State University, 420008 Kazan, Russia Federation
E-mail: boris.malkin@ksu.ru

R. S. Meltzer (Chapter 4) — Department of Physics and Astronomy, University of Georgia, Athens, GA 30602, USA
Tel. 706 542 5515, Fax 706 542 2492
E-mail: rmeltzer@hal.physast.uga.edu

F. Auzel
(Chapter 5)
Centre National de la Recherche Scientifique, GOTR, UMR 7574, France
E-mail: francois. auzel@wanadoo. fr

R. Moncorgé
(Chapter 6)
CIRIL, UMR 6637 CNRS-CEA-ISMRA, Université de Caen, 6 Boulevard Maréchal Juin, 14050 Caen, France
E-mail: moncorge@spalp255. ismra. fr

Y. C. Sun
(Chapter 7)
Physics Department, Montana State University, Bozeman, Montana 59717, USA
Tel. 406 994 6163, Fax 406 994 4452
E-mail: sun@physics. montana. edu

B. Jacquier
(Chapter 8)
B. Jacquier, L. Bigot, S. Guy, A. M. Jurdyc
University Claude Bernard Lyon 1
Villeurbanne F-69622, France

J. -C. G. Bünzli
(Chapter 9)
Chemistry Department, University of Lausanne, BCH 1402, Lausanne, CH-1015, Switzerland
Tel. 41 21 692 3821, Fax 41 21 692 3825
E-mail: Jean-claude. bunzli@icma. unil. ch

M. Z. Su
(Chapter 10)
College of Chemistry and Molecular Engineering, Peking University, Beijing, 100871, China
Tel. 86 10 6275 1715, Fax 86 10 6275 1708
E-mail: sumz@pku. edu. cn

W. Zhao
(Chapter 10)
Department of Chemistry, University of Arkansas, 2801 South University Ave. Little Rock, AR 72204, USA
E-mail: wxzhao@ualr. edu

1 Electronic Energy Level Structure

Guokui Liu

1.1 Introduction

From fluorescent lamps, solid-state lasers, to optical amplifiers in fiber optics, rare earth (RE) elements, or lanthanides, have been widely used to activate luminescent and photonic materials. A majority of applications involve electronic transitions between states within a $4f^N$ configuration of trivalent (or divalent) RE ions doped into transparent host materials. The popular solid-state laser of Nd^{3+}: YAG, for example, utilizes the 1.05-μm electronic transition from the $^4F_{3/2}$ to $^4I_{11/2}$ multiplets within the $4f^3$ configuration of the Nd^{3+} ion (see Chapter 6). Similarly, the Er^{3+} fluorescence at 1.5-μm, emitted from the first excited multiplet $^4I_{13/2}$ of the $4f^{11}$ configuration, is important because of its high quantum efficiency and optimal wavelength for optical amplification in telecommunications. Green fluorescence of Er^{3+} from the $^4S_{3/2}$ state can be induced through up-conversion excitation from several states at lower energies (see Chapter 5). These applications utilize the unique properties of the 4f electrons that have localized states and exhibit weak coupling to ligand electrons and lattice vibrations. The 4f spectroscopic properties, including the energy level structure and the dynamics of the electronic transitions of RE ions in solids, thus primarily define the optical properties of an RE activated device.

With energy levels at more than 30,000 cm^{-1} above the ground states of the $4f^N$ configurations, there are 5d, 6s, 6p orbitals in the RE ion electronic structure. The 5d states exhibit less localized nature and stronger coupling to lattice vibrations, and since the inter-configuration $4f^N$ to $4f^{N-1}5d$ transitions of the RE ions are parity-allowed, they have intensities up to 10,000 times stronger than the strongest $4f^N$ to $4f^N$ transitions (see Chapter 2). Due to these electronic properties, $4f^N$ to $4f^{N-1}5d$ transitions have become increasingly important in recent years for applications in fast scintillators and ultraviolet laser sources. A fundamental understanding of the electronic energy levels of RE ions in the $4f^N$ and $4f^{N-1}5d$ configurations is essential not only in spectroscopy but also in materials characterization.

What appears to be unique in solid-state RE spectroscopy is that the electronic energy level structure is established primarily using the quantum theory of atomic spectroscopy, and all collective solid-state effects can be treated as a perturbation known as the crystal-field interaction (Stevens, 1952; Wybourne, 1965; Newman and Ng, 2000). Such a simple approximation works very well

for RE ions in a $4f^N$ configuration in which the electrons in the partially occupied 4f shell are shielded by the electrons in the 5s and 5p shells from interacting with the ligands and, therefore, have little participation in chemical bond formation (Reisfeld and Jφrgensen, 1977). Figure 1.1 shows, with Nd^{3+} as an example, the radial distribution of electrons in different shells. It is clear that most of the 4f orbitals are much less extended than the 5s and 5p orbitals. As a result, the electronic transitions between the 4f states are very sharp and have atomic-like spectral characteristics. It is based on the localized nature of the electronic properties that a general theoretical framework of solidstate RE spectroscopy was developed (Stevens, 1952; Judd, 1963a; Wybourne, 1965; Dieke, 1968).

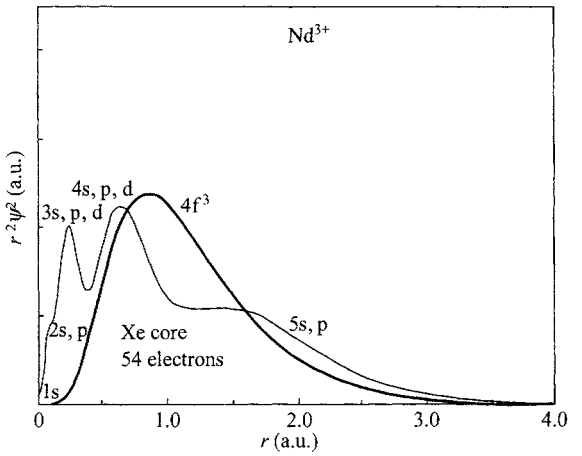

Figure 1.1 Radial wave function $r^2\psi^2$ as a function of r in atomic radius for $4f^3$ electrons of Nd^{3+} in comparison with the charge distribution of its core (Xe) configurations

When a 4f electron is excited into a 5d orbital that extends beyond the 5s and 5p orbitals, the spectroscopic properties of RE ions in an electronic configuration such as $4f^{N-1}$ 5d are influenced more strongly by the lattice. Therefore, the electronic transitions between the $4f^N$ and $4f^{N-1}5d$ states, through absorption or emission of photons, are expected to be characteristically very different from transitions within the $4f^N$ configuration. A modification of the crystal-field theory is necessary for modeling stronger ion-lattice interactions in analysis of the energy level splitting and the excited state dynamics.

With restrictions on localized electronic interactions in a well-defined crystalline environment, the overall spectroscopic properties of an RE ion may be determined by evaluating interactions in various forms of mechanisms. Table 1.1 lists the scales of electronic energy levels in terms of different mechanisms of electronic interactions. Accordingly, theoretical analyses of the electronic interactions and their contribution to energy level splitting will be discussed in the

order of energy level scales. Historically, the development of a complete Hamiltonian for $4f^N$ configurations was approached in two stages. The first dealt with the fundamental electronic interactions, including electrostatic Coulomb interactions and spin-orbit coupling. The second dealt with the crystal field interaction that arises when the ion is in a condensed phase. Subsequently, additional effective operators dealing with higher order free-ion interactions and corrective crystal-filed interactions were introduced to reproduce more accurately the energy level structures observed in experiments. The theoretical framework, thus utilizes well-established theories in two conventional fields: (1) the quantum theory of atomic spectroscopy that is the foundation for establishing free-ion energy level structures; (2) the point group theory that facilitates the determination of crystal-field splittings according to the symmetry properties of a crystalline lattice.

As listed in Table 1.1, the scale of crystal-field splitting is smaller than that of the free-ion splitting, while the hyperfine energy level structures are even smaller, thus ensuring the legitimate application of perturbation theory to calculations of crystal-field splitting and hyperfine structures. In the framework of crystal-field modeling, electronic energy levels are calculated by diagonalizing an effective-operator Hamiltonian with the basis free-ion wave functions, and the parameters of the effective operators are determined by fitting the experimentally observed energy levels to the calculated ones. As an empirical approach to modeling the energy level structure of RE ions in solids, crystal-field theory was very successful not only in predicting the exact number of crystal-field levels for an RE ion in a given host material, but also in accurately determining their energies.

Table 1.1 Energy level scales of rare earth ions in crystals

Interaction Mechanism	Energy (cm^{-1})	Optical Probe
Configuration splitting ($4f^N - 4f^{N-1}\,5d$)	10^5	UV and VUV spectroscopy
Splitting within a $4f^N$ configuration		
Non-central electrostatic field	10^4	Absorption, fluorescence or laser excitation spectroscopy
Spin-orbit interaction	10^3	
Crystal field interaction	10^2	
Ion-ion interaction induced band structure (in stoichiometric compounds)	$10^{-2} - 10$	
Hyperfine splitting	$10^{-3} - 10^{-1}$	Selective and nonlinear laser spectroscopy
Superhyperfine splitting (ion-ligand hyperfine interaction)	$10^{-4} - 10^{-2}$	

In this chapter, we discuss the electronic energy level structure of RE ions in crystalline solids. Given that the theoretical foundation has already be established and discussed comprehensively in several books (Judd, 1963a; Wybourne, 1965; Dieke 1968; Abragam and Bleaney, 1986; Hüfner, 1978; Weissbluth, 1978; Cowan, 1981; Newman and Ng, 2000), we will not enter into details of

the spectroscopic theory. Instead, an overview of modeling the electronic energy level structure of RE ions in dielectric crystals is provided. An effective operator Hamiltonian is introduced with tensor operators defined according to the nature of electronic interactions. The terms of Hamiltonian include free-ion interactions such as electrostatic Coulomb interactions and spin-orbit coupling, the ion-ligand interactions described in the framework of crystal-field theory, and the hyperfine interactions treated as a perturbation on electronic energy levels. Solutions to the Hamiltonian are obtained primarily through empirical approaches in which the phenomenological parameters of the effective operators of the Hamiltonian are determined. The calculations of the electronic energy level structures of RE ions require complicated tensor operation and the theory of angular momentum coupling (Judd, 1963a; Weissbluth, 1978; Cowan, 1981). In Appendices A and B of this book, properties of tensor operators, particularly the effective-operator Hamiltonian, and angular momentum coupling are briefly discussed.

Spectroscopic studies of magnetic and hyperfine interactions of RE ions in solids are an important part of solid-state RE spectroscopy and have gained significant applications in both fundamental understanding of physical interactions and materials characterization (see Chapters 4, 5 and 7). The advances in high resolution and nonlinear laser spectroscopic techniques have facilitated the measurements of RE hyperfine energy levels in great detail (Levenson, 1982; Macfarlane and Shelby, 1987). In Section 1.6, we discuss various mechanisms of hyperfine interactions and Zeeman effect. Their contributions to energy level splittings from the GHz to the kHz spectral range are evaluated on the same basis of crystal-field interaction.

It is the author's intention to outline the practical procedures of analyzing experimental spectra and, at the same time, to provide the reader a clear theoretical understanding of the electronic interactions, including crystal-field and hyperfine interactions of RE ions in crystals. In this regard, this chapter may stand alone as a useful guide to chemists and materials scientists in analysis of RE spectra. However, more importantly, this chapter serves as an introduction to other chapters, which assume the reader's understanding of the concepts of electronic interactions and the RE energy level structures.

1.2 Electronic States and Coupling Schemes

1.2.1 Central Field Approximation

A conventional approach to solving Schrödinger equation for an N-electron atomic system is to use the central field approximation and Hartree-Fock method (Hartree, 1957; Slater, 1960; Weissbluth, 1978). In the central field approximation, each electron is assumed to move independently in the field of the nucleus and a central field that is made up of the spherically averaged

potential fields of each of the other electrons. The quantum mechanical solution for such a central field system is the same as that for a single electron hydrogen atom. With the concept of central field approximation, the non-spherical part of the electronic interactions is treated as a perturbation to a spherically symmetric potential, so that the basis of the hydrogen atom wave functions can be used to construct wave functions for an N-electron atom (ion). This method has been used to classify electronic states and evaluate energy levels of lanthanide and actinide ions (Judd, 1963a; Wybourne, 1965).

The primary terms of the Hamiltonian for an N-electron ion in the absence of external fields is commonly expressed as

$$\mathscr{H} = \mathscr{H}_0 + \mathscr{H}_C + \mathscr{H}_{SO} \tag{1.1}$$

where

$$\mathscr{H}_0 = -\sum_{i=1}^{N} \frac{\hbar^2}{2m} \nabla_i^2 - \sum_{i=1}^{N} \frac{Ze^2}{r_i}, \tag{1.2}$$

$$\mathscr{H}_C = \sum_{i<j}^{N} \frac{e^2}{r_{ij}}, \tag{1.3}$$

$$\mathscr{H}_{SO} = \sum_{i}^{N} \xi(r_i) \boldsymbol{l}_i \cdot \boldsymbol{S}_i. \tag{1.4}$$

In Eq. (1.2), the first term is the kinetic energy, and the second term is the potential energy of the electrons in the field of the nucleus, which is purely radial and contributes energy shifts that are the same for all the levels belonging to a configuration without affecting the energy level structure of the configuration. In Eq. (1.3), the term $\mathscr{H}_C$ represents the inter-electron Coulomb repulsion between a pair of electrons at a distance of r_{ij}, which varies for different states of the same configuration. In Eq. (1.4), the term $\mathscr{H}_{SO}$ describes the spin-orbit interactions, which can be understood as magnetic dipole-dipole interactions between the spin and angular moment of the electrons. The spin-orbit coupling constant $\xi(r_i)$ is defined as a sole function of r_i.

Exact solutions of Schrödinger equation are not possible for systems with more than one electron. In the framework of the central field approximation, one assumes that it is possible to construct a potential energy function $U(r_i)$ which is a spherically symmetric, one-electron operator and is a good approximation to the actual potential energy of the electron i in the field of the nucleus and the other $N-1$ electrons. Therefore, $\mathscr{H}_0$ can be replaced by (Weissbluth, 1978)

$$\mathscr{H}_0' = \sum_{i=1}^{N} \left[-\frac{\hbar^2}{2m} \nabla_i^2 + U(r_i) \right], \tag{1.5}$$

with

$$\sum_{i=1}^{N} U(r_i) = -\sum_{i=1}^{N} \frac{Ze^2}{r_i} + \left\langle \sum_{i<j}^{N} \frac{e^2}{r_{ij}} \right\rangle. \tag{1.6}$$

The second term in Eq. (1.6) is the average over a sphere of the electron repulsion. This term is therefore independent of the angular coordinates. $\mathscr{H}'_0$ contains the kinetic energy, the potential energy of N electrons, and most of the inter-electron repulsion, and it is called the Hamiltonian of the central field. Since most of the inter-electron repulsion is included in the central field Hamiltonian of Eq. (1.5), the second term in Eq. (1.1) can be rewritten as

$$\mathscr{H}'_C = \sum_{i<j}^{N} \frac{e^2}{r_{ij}} - \left\langle \sum_{i<j}^{N} \frac{e^2}{r_{ij}} \right\rangle, \tag{1.7}$$

which is small enough to be treated along with the spin-orbit Hamiltonian (1.4) as a perturbation to the central field potential.

The eigenfunctions of $\mathscr{H}'_0$ for an N-electron ion are obtained as a linear combination of one-electron Vave functions that satisfy the Pauli exclusion principle and are subject to the orthonormalty condition. This method, known as Hartree-Fock approach, is generally used for seeking an approximate solution to the N-electron Schrödinger equation (Hartree, 1957; Weissbluth, 1978). The effects of non-central field interactions including spin-orbit coupling and many-body electronic interactions are considered by introducing additional effective operators and diagonalizing the Hamiltonian with parameters determined in comparison with experiments.

In the Hartree-Fock method, the wave function of each electron is expressed as a product of radial and angular functions of the spherical harmonics multiplied by a spin function

$$\Psi_{nlm_lm_s}(\boldsymbol{r}, m_s) = \frac{1}{r} R_{nl}(r) Y_{lm_l}(\theta, \varphi) \sigma(m_s), \tag{1.8}$$

where the radial function $R_{nl}(r)$ depends on the central field potential, which determines the radial charge distribution functions such as those plotted in Fig. 1.1 for Nd^{3+}. The spherical harmonic function $Y_{lm_l}(\theta, \varphi)$ in Eq. (1.8) is characterized by the four quantum numbers n, l, m_l and m_s, which define a unique state of an electron in an atom. For electrons in a $4f^N$ cnfiguration, we have

$$\begin{aligned} &n = 4, \\ &l = 3, \ m_l = -l, -l+1, \cdots, l, \\ &m_s = \pm 1/2. \end{aligned} \tag{1.9}$$

The central field wave function for N-electrons thus may be written in a

determinantal form as

$$\Psi(\lambda_1, \lambda_2, \cdots, \lambda_N) = \frac{1}{\sqrt{N!}} \begin{vmatrix} \psi_1(\lambda_1) & \psi_2(\lambda_1) & \cdots & \psi_N(\lambda_1) \\ \psi_1(\lambda_2) & \psi_2(\lambda_2) & \cdots & \psi_N(\lambda_2) \\ \vdots & & & \\ \psi_1(\lambda_N) & \psi_2(\lambda_N) & \cdots & \psi_N(\lambda_N) \end{vmatrix}, \quad (1.10)$$

in which $\psi_i(\lambda_j)$ are spin orbitals. The subscript i identifies a particular choice of the four quantum numbers n, l, m_l, and m_s, where λ_j represents the space and spin coordinates of the j-th electron. The primary purpose of the central field approximation is to use the N-electron wave functions defined by Eq. (1.10) as the basis functions for the perturbation terms such as the inter-electron Coulomb interactions [see Eq. (1.7)] and spin-orbit interaction [see Eq. (1.4)] of the Hamiltonian.

1.2.2 *LS* Coupling and Intermediate Coupling

To construct wave functions for a multi-electron atom on the basis of the central field approximation, one needs to choose a coupling scheme of momentum summation to determine the wave functions of the N-independent electrons. There are two coupling schemes that are commonly used for two extreme cases in atomic spectroscopy (Judd, 1963a; Cowan, 1981). In lighter atoms, where spin orbit interactions [see Eq. (1.4)] tend to be small compared with the electrostatic interactions between electrons [see Eq. (1.3)], the so-called Russell-Saunders, or *LS* coupling scheme is a good choice, since L and S are, approximately, good quantum numbers. With increasing Z, electrostatic interactions decrease and spin-orbit interactions become more important. In the heavier atoms, spin-orbit interactions become much stronger than the Coulomb interactions. Thus, one should consider the *j-j* coupling scheme. In rare earth ions, the Coulomb electrostatic interactions and spin-orbit interactions have the same order of magnitudes. Therefore, neither coupling scheme is appropriate, and calculations of energy levels of RE ions are mathematically more involved in a scheme called intermediate coupling, which can be developed from the *LS* scheme.

In the *LS* coupling scheme, orbital momentum and spin momentum of individual electrons are summed separately (Weissbluth, 1978). Thus

$$\boldsymbol{L} = \sum_{i=1}^{N} \boldsymbol{l}_i, \quad \boldsymbol{S} = \sum_{i=1}^{N} \boldsymbol{s}_i, \quad (1.11)$$

are the total orbit and total spin momentum operators, respectively, and

$$\boldsymbol{J} = \boldsymbol{L} + \boldsymbol{S}, \quad (1.12)$$

is the total angular momentum operator which has $2J + 1$ eigenstates represented

by the magnetic quantum number $M = -J, -J+1, \cdots, J$.

In the *LS* coupling scheme, the electronic states of an RE ion may be specified completely by writing the basis states as

$$\Psi = |nl\tau LSJM\rangle, \tag{1.13}$$

where *nl*, which is 4f, or 5d for RE ions, represents the radial part of the basis states. Usually, the symbol $^{2S+1}L_J$ is used for naming a free ion state or multiplet. Whereas *S* and *J* are specified with numbers (0, 1/2, 1, ···), *L* is traditionally specified with letters *S, P, D, F, G, H,* ···, respectively, for *L* = 0, 1, 2, 3, 4, 5, ··· Table 1.2 lists the electronic configurations and ground states identified by $^{2S+1}L_J$ for divalent and trivalent ions in the RE series.

Table 1.2 Electronic configurations and ground states of divalent (R^{2+}) and trivalent (R^{3+}) RE ions

Atomic number	Element		R^{2+}	R^{3+}
57	La	Lanthanum	$4f^1$, $^2F_{5/2}$	$4f^0$, $^1S_0$
58	Ce[a]	Cerium	$4f^2$, $^3H_4$	$4f^1$, $^2F_{5/2}$
59	Pr[a]	Praseodymium	$4f^3$, $^4I_{9/2}$	$4f^2$, $^3H_4$
60	Nd	Neodymium	$4f^4$, $^5I_4$	$4f^4$, $^4I_{9/2}$
61	Pm	Promethium	$4f^5$, $^6H_{5/2}$	$4f^4$, $^5I_4$
62	Sm	Samarium	$4f^6$, $^7F_0$	$4f^5$, $^6H_{5/2}$
63	Eu	Europium	$4f^7$, $^8S_{7/2}$	$4f^6$, $^7F_0$
64	Gd	Gadolinium	$4f^8$, $^7F_6$	$4f^7$, $^8S_{7/2}$
65	Tb[a]	Terbium	$4f^9$, $^6H_{15/2}$	$4f^8$, $^7F_6$
66	Dy	Dysprosium	$4f^{10}$, $^5I_8$	$4f^9$, $^6H_{15/2}$
67	Ho	Holmium	$4f^{11}$, $^4I_{15/2}$	$4f^{11}$, $^5I_8$
68	Er	Erbium	$4f^{12}$, $^3H_6$	$4f^{11}$, $^4I_{15/2}$
69	Tm	Thulium	$4f^{13}$, $^2F_{7/2}$	$4f^{12}$, $^3H_6$
70	Yb	Ytterbium	$4f^{14}$, $^1S_0$	$4f^{13}$, $^2F_{7/2}$
71	Lu	Lutecium	$4f^{14}6s$, $^2S_{1/2}$	$4f^{14}$, $^1S_0$

(a) Ce, Pr and Tb may also be stabilized in tetravalent oxidation states. The electronic configuration and ground state of RE in tetravalent oxidation state can be determined from this table. For example, Pr^{4+} is in $4f^1$ ($^2F_{5/2}$) configuration (state).

An additional quantum number τ, called the seniority number, is needed for distinguishing the states that have the same *L* and *S* quantum numbers. In fact, two or more quantum numbers are needed in order completely to define the states in an f^N configuration. One such classification number is $W = (w_1 w_2 w_3)$, with three integers for characterizing the irreducible representations of the seven-dimenisional rotational group R_7. The other classification number is $U = (u_1 u_2)$, for characterizing the irreducible representations of the group G_2. Details in classification of the f^N states are given in the books by Judd (1963a) and Wybourne (1965). Table 1.3 lists the classification of the states for the f^N

Table 1.3 Classification of the free ion states of the f^N configurations (Wybourne, 1965)

N	τ	W	U	^{2S+1}L	N_J	N	τ	W	U	^{2S+1}L	N_J
1	1	(100)	(10)	^{2}F	2	5	(221)		(10)	^{2}F	2
2	2	(110)	(10)	^{3}F	3				(11)	^{2}PH	4
			(11)	^{3}PH	6				(20)	^{2}DGI	6
	2	(200)	(20)	^{1}DGI	3				(21)	^{2}DFGHKL	12
	0	(000)	(00)	^{1}S	1				(30)	^{2}PFGHIKM	14
3	3	(111)	(00)	^{4}S	1				(31)	^{2}PDFFGHHIIKK-LMNO	30
			(10)	^{4}F	4						
			(20)	^{4}DGI	12		3	(210)	(11)	^{2}PH	4
	3	(210)	(11)	^{2}PH	4				(20)	^{2}DGI	6
			(20)	^{2}DGI	6				(21)	^{2}DFGHKL	12
			(21)	^{2}DFGHKL	12		1	(100)	(10)	^{2}F	2
	1	(100)	(10)	^{2}F	2	6	6	(100)	(10)	^{7}F	7
4	4	(111)	(00)	^{5}S	1		6	(210)	(11)	^{5}PH	8
			(10)	^{5}F	5				(20)	^{5}DGI	15
			(20)	^{5}DGI	15				(21)	^{5}DFGHKL	30
	4	(211)	(10)	^{3}F	3		4	(111)	(00)	^{5}S	1
			(11)	^{3}PH	6				(10)	^{5}F	5
			(20)	^{3}DGI	9				(20)	^{5}DGI	15
			(21)	^{3}DFGHKL	18		6	(221)	(10)	^{3}F	3
			(30)	^{3}PFGHIKM	21				(11)	^{3}PH	6
	2	(110)	(10)	^{3}F	3				(20)	^{3}DGI	9
			(11)	^{3}PH	6				(21)	^{3}DFGHKL	18
	4	(220)	(20)	^{1}DGI	3				(30)	^{3}PFGHIKM	21
			(21)	^{1}DFGHKL	6				(31)	^{3}PDFFGHHIIKKLMNO	45
			(22)	^{1}SDGHILN	7		4	(211)	(10)	^{3}F	3
	2	(200)	(20)	^{1}DGI	3				(11)	^{3}PH	6
	0	(000)	(00)	^{1}S	1				(20)	^{3}DGI	9
5	5	(110)	(10)	^{6}F	6				(21)	^{3}DFGHKL	18
			(11)	^{6}PH	9				(30)	^{3}PFGHIKM	21
	5	(211)	(10)	^{4}F	4		2	(110)	(10)	^{3}F	3
			(11)	^{4}PH	7				(11)	^{3}PH	6
			(20)	^{4}DGI	12		6	(222)	(00)	^{1}S	1
			(21)	^{4}DFGHKL	24				(20)	^{1}DGL	3
			(30)	^{4}PFGHIKM	27				(30)	^{1}PFGHIKM	7
	3	(111)	(00)	^{4}S	1				(40)	^{1}SDFGGHIIKLLMNQ	14
			(10)	^{4}F	4		4	(220)	(20)	^{1}DGI	3
			(20)	^{4}DGI	12				(21)	^{1}DFGHKL	6

continue

N τ	W	U	^{2S+1}L	N_J	N τ	W	U	^{2S+1}L	N_J
		(22)	^{1}SDGHILN	7	7	(222)	(00)	^{2}S	1
2	(200)	(20)	^{1}DGI	3			(10)	^{2}F	2
0	(000)	(00)	^{1}S	1			(20)	^{2}DGI	6
7 7	(000)	(00)	^{8}S	1			(30)	^{2}PFGHIKM	14
7	(200)	(20)	^{6}DGI	17			(40)	^{2}SDFGGHIIKL-	27
5	(110)	(10)	^{6}F	6				LMNQ	
		(11)	^{6}PH	9	5	(221)	(10)	^{2}F	2
7	(220)	(20)	^{4}DGI	12			(11)	^{2}PH	4
		(21)	^{4}DFGHKL	24			(20)	^{2}DGI	6
		(22)	^{4}SDGHILN	25			(21)	^{2}DFGHKL	12
5	(211)	(10)	^{4}F	4			(30)	^{2}PFGHIKM	14
		(11)	^{4}PH	7			(31)	^{2}PDFFGHHIIKK-	30
		(20)	^{4}DGI	12				LMNO	
		(21)	^{4}DFGHKI	24	3	(210)	(11)	^{2}PH	4
		(30)	^{4}PFGHIKM	27			(20)	^{2}DGI	6
3	(111)	(00)	^{4}S	1			(21)	^{2}DFGHKL	12
		(10)	^{4}F	4	1	(100)	(10)	^{2}F	2
		(20)	^{4}DGI	12					

configurations with $N \leqslant 7$. Column 5 lists the LS terms with the same S, and Column 6 lists the number of $^{2S+1}L_J$ multiplets in the classification. The LS terms of the $4f^{14-N}$ configuration are identical for those of the $5f^N$ configuration with $N>7$, although the seniority of the states is different.

In the LS coupling scheme, the spin-orbit interaction Hamiltonian commutes with $\boldsymbol{J}^2$ and J_z, but not with $\boldsymbol{L}$ and $\boldsymbol{S}$:

$$\begin{aligned} &[\mathscr{H}_{SO}, \boldsymbol{L}] \neq 0, [\mathscr{H}_{SO}, \boldsymbol{S}] \neq 0, \\ &[\mathscr{H}_{SO}, \boldsymbol{J}^2] = [\mathscr{H}_{SO}, J_z] = 0, \end{aligned} \tag{1.14}$$

which means that inclusion of spin-orbit coupling breaks the symmetry of the LS coupling scheme. In this case, L and S are no longer good quantum numbers, but J and M are still good. The wave functions $|nl\tau LSJM\rangle$ are not eigenfunctions of the Hamiltonian of Eq. (1.1). Based on perturbation theory and the concept of the central field approximation, one may obtain a new set of eigenfunctions by diagonalizing the primary terms of the Hamiltonian defined by Eqs. (1.4) and (1.7) with the basis of $|nl\tau LSJM\rangle$. As a result, the new eigenfunctions are linear combinations of the LS basis sets, and are known as the free-ion wave

functions in the intermediate coupling scheme. If we do not include inter-configurational coupling, the eigenfunctions in the intermediate coupling scheme are expressed as

$$\Psi(nlJ) = \sum_{\tau LS} a_{\tau LSJ} |nl\tau LSJ\rangle, \tag{1.15}$$

where the coefficients $a_{\tau LSJ}$ are determined by the matrix elements,

$$a_{\tau LSJ} = \sum_{\tau' L' S'} \langle nl\tau LSJ | \mathscr{H}_{\mathrm{C}} + \mathscr{H}_{\mathrm{SO}} | nl\tau' L' S' J' \rangle \delta_{JJ'}. \tag{1.16}$$

The energy levels of the free-ion states are independent of M, so they are $(2J+1)$-fold degenerate. The new basis Eq. (1.15) in the intermediate coupling scheme describes the energy states of the Hamiltonian including Coulomb and spin-orbit interactions and is obtained from mixing all LS terms with the same J in a given $4f^N$ configuration. The transformation coefficients of $a_{\tau SLJ}$ are the components of the eigenvector pertaining to the basis state in the LS coupling (Judd, 1963).

1.3 Free-ion Interactions

In spectroscopy, a powerful method for evaluating atomic energy level structure (or RE ion energy level structure in our case) is to define and diagonalize an effective-operator Hamiltonian with the wave functions of the central field Hamiltonian. Racah (1949) used this method for calculating the energy matrix elements of the tensor operators of the electronic angular momentum. Since then, many developments have been made, particularly for applications of the effective operator method to rare earth spectroscopy (Judd, 1963a; Wybourne, 1965). In this section, we will review the primary results of the theory that are important for understanding the free-ion properties of RE ions in solids. The effective operator Hamiltonian and its reduced matrix elements for the Coulomb electrostatic interaction and spin-orbit coupling are discussed, while the effective operators for higher order free-ion interactions are presented without derivations. An essential part of the effective operator method is to determine the irreducible matrix elements of tensor operators using the Wigner-Eckart theorem (see B.9 in Appendix B). For more comprehensive theories of tensor operators and atomic spectroscopy, one may read textbooks by Judd (1963a) and Weissbluth (1978).

1.3.1 Coulomb Interaction

In the central field approximation, orbital electronic wave functions of an RE ion

are represented by products of radial and angular parts as shown in Eq. (1.8). The effective operator for Coulomb electrostatic intra-ion interaction may be expressed by expanding $1/r_{ij}$ into scalar products of the tensor operators of spherical harmonics as follows:

$$\frac{1}{r_{ij}} = \sum_{k=0}^{\infty} \frac{4\pi}{2k+1} \frac{r_<^k}{r_>^{k+1}} \mathrm{Y}_i^{(k)} \cdot \mathrm{Y}_j^{(k)}, \tag{1.17}$$

where $r_<$ indicates the distance from the nucleus to a near electron, and $r_>$ the distance from the nucleus to a further electron, and

$$\mathrm{Y}^{(k)}(i) \cdot \mathrm{Y}^{(k)}(j) = \sum_{-k \leqslant q \leqslant k} (-1)^q \mathrm{Y}_q^{(k)}(\theta_i, \varphi_i) \mathrm{Y}_{-q}^{(k)}(\theta_j, \varphi_j). \tag{1.18}$$

It is convenient to define a tensor $\boldsymbol{C}^{(k)}$ as (Weissbluth, 1978)

$$\boldsymbol{C}^{(k)} = \sqrt{\frac{4\pi}{2k+1}} \mathrm{Y}^{(k)} \tag{1.19}$$

with components given in Appendix B Eq. (B.12). The reduced matrix elements of $\boldsymbol{C}^{(k)}$ may be expressed as

$$\left\langle l \| \boldsymbol{C}^{(k)} \| l' \right\rangle = (-1)^l [(2l+1)(2l'+1)]^{1/2} \begin{pmatrix} l & k & l' \\ 0 & 0 & 0 \end{pmatrix}. \tag{1.20}$$

The 3-j symbol in Eq. (1.20) is defined in Eq. (B.6) in Appendix B. Therefore, for N equivalent electrons in orbital nl, the matrix of the effective operator Hamiltonian for Coulomb electrostatic interaction may be expressed as

$$\left\langle l^N \tau LS \left| \sum_{i>j}^{N} \frac{e^2}{r_{ij}} \right| l^N \tau LS \right\rangle = \sum_k f_k(l, l) F^k(nl, nl), \tag{1.21}$$

where $F^k(nl, nl)$, with $k = 0, 2, 4, 6$, are the Slater radial integrals for the radial part of the electrostatic interaction, which is defined as

$$F^k(nl, nl) = e^2 \int_0^\infty \int_0^\infty \frac{r_<^k}{r_>^{k+1}} [R_{nl}(r_i)]^2 [R_{nl}(r_j)]^2 \mathrm{d}r_i \mathrm{d}r_j. \tag{1.22}$$

The value of F^k may be calculated using the Hartree-Fock method, but in actual cases of spectrum analysis, F^k is considered an experimentally determined parameter. The angular part of matrix (1.21) is defined as

$$f_k(l,l) = \left\langle l^N\tau LS \middle| \sum_{i>j} \boldsymbol{C}^{(k)}(i)\cdot\boldsymbol{C}^{(k)}(j) \middle| l^N\tau LS \right\rangle. \quad (1.23)$$

The matrix elements (1.23) are best handled by introducing the unit tensor operator $\boldsymbol{U}^{(k)}$ (Weissbluth, 1978) with reduced matrix elements expressed in Appendix B Eqs. (B.10) and (B.11). In combination with symmetry properties of angular momentum, $f_k(l,l)$ may be expressed in terms of the reduced matrix elements of $\boldsymbol{U}^{(k)}$ as

$$f_k(l,l) = \frac{1}{2}(2l+1)^2\begin{pmatrix} l & k & l \\ 0 & 0 & 0 \end{pmatrix}^2 \times\left\{\frac{1}{2L+1}\sum_{\tau L'}\left|\left\langle l^N\tau LS \| \boldsymbol{U}^{(k)} \| l^N\tau' L'S'\right\rangle\right|^2 - \frac{N}{2l+1}\right\}. \quad (1.24)$$

In the particular case of $k=0$, it is easy to find that

$$f_0(l,l) = N(N-1)/2. \quad (1.25)$$

For the p^N, d^N, and f^N configurations, the values for the reduced matrix elements of the tensor operator $\boldsymbol{U}^{(k)}$ were tabulated by Nielson and Koster (1963), and may also be displayed in SPECTRA program. Because of the symmetry properties of the 3-j symbol, the matrix in Eq. (1.24) has nonzero elements only if $l+l\geqslant k\geqslant|l-l|$, and k must be even. For the 4f electrons, $l=3$, thus the f_k matrix vanishes except for $k=0,2,4,6$.

To illustrate the use of the reduced matrix elements for energy level calculation in the simple case of f^3 configuration (Nd^{3+}), Table 1.4 lists the values of electrostatic matrix elements in terms of F^k along with other free-ion interaction parameters to be introduced in the Section 1.3.2 and 1.3.3.

Table 1.4 Elements of the $J=1/2$ submatrix of the free-ion Hamiltonian for f^3 configurations (in the first and second columns, 1 stands for ^4D and 2 for ^2P)

Ψ	Ψ'	Coefficient	Parameter
1	1	1.00000000	E_0
2	2	1.00000000	E_0
1	1	0.17264957	F^2
2	2	−0.04957265	F^2
1	1	0.01165501	F^4
2	2	0.00155400	F^4
1	1	−0.19873289	F^6
2	2	0.07321738	F^6
1	1	−0.02446153	0.01α
2	2	−0.02846153	0.01α
1	1	−0.10256410	β

continue

Ψ	Ψ'	Coefficient	Parameter
2	2	-0.26923077	β
1	1	-0.32307690	γ
2	2	0.27692306	γ
1	1	1.11116780	T^2
2	2	-0.25253800	T^2
1	1	0.09759000	T^3
2	2	-0.58554000	T^3
1	1	-1.16700680	T^4
2	2	-1.52362350	T^6
1	1	-1.50000000	ζ
1	1	11.89999944	M^0
1	1	-18.09999640	M^2
1	1	-19.40908767	M^4
1	1	-0.12777776	P^2
1	1	-0.04292929	P^4
1	1	0.03399380	P^6
1	2	-1.58113883	ζ
1	2	-2.42441266	M^0
1	2	2.31900337	M^2
1	2	-0.81452561	M^4
1	2	0.06441676	P^2
1	2	0.01597110	P^4
1	2	-0.03583260	P^6
2	2	4.66666625	M^0
2	2	3.00000097	M^2
2	2	-6.36363739	M^4
2	2	-0.09629627	P^2
2	2	0.07575757	P^4
2	2	-0.04532506	P^6

1.3.2 Spin-orbit Interaction

As defined in Eq. (1.4), the Hamiltonian the for spin-orbit coupling of N electrons in a rare earth ion is a linear summation of independent spin-orbit interactions for a single electron. In LS coupling, the N equivalent electron matrix elements of the spin-orbit interaction are expressible in terms of tensor operator $\boldsymbol{V}^{(11)}$, so that the matrix element of spin-orbit interaction for N equivalent electrons can be expressed as (Sobelman, 1972; Weissbluth, 1978)

$$\left\langle nl^N \tau LSJM \left| \sum_{i=1}^{N} \xi(r_i) \boldsymbol{l}_i \cdot \boldsymbol{S}_i \right| nl^N \tau' L'S'J'M' \right\rangle = \zeta_{nl} A_{SO}(nl), \quad (1.26)$$

where ζ_{nl} is the spin-orbit interaction parameter which is a radial integral defined by

$$\zeta_{nl} = \int_0^\infty [R_{nl}(r)]^2 \xi(r)\, \mathrm{d}r. \quad (1.27)$$

The spin-orbit parameter can be evaluated numerically using the Hartree-Fock central field potential, but it is usually adjusted to the experimentally observed energies. The matrix element in Eq. (1.26) can be expressed as

$$\begin{aligned} A_{SO}(nl) &= (-1)^{L+S'+J} \sqrt{(2l+1)(l+1)l}\,\delta_{JJ'}\delta_{MM'} \\ &\times \begin{Bmatrix} L & S & J \\ S' & L' & 1 \end{Bmatrix} \langle \tau LS \| \boldsymbol{V}^{(11)} \| \tau' L'S' \rangle, \end{aligned} \quad (1.28)$$

where $\{\ldots\}$ is a 6-j symbol. The values for the reduced matrix elements of the tensor operator $\boldsymbol{V}^{(11)}$ are tabulated in the books by Sobelman (1972) and Nielson and Koster (1963). They may be output from the SPECTRA program.

1.3.3 Corrections to Free-ion Hamiltonian

The electrostatic and spin-orbit interactions give the right order for the energy level splitting of the f^N configurations. However, these primary terms of the free ion Hamiltonian do not accurately reproduce the experimentally measured energy level structures. This is because the parameters F^k and ζ_{nf}, which are associated with interactions within a f^N configuration, cannot absorb all the effects of additional mechanisms such as relativistic effects and configuration interactions. Introduction of new terms to the effective operator Hamiltonian is required to better interpret the experimental data. Judd and Crosswhite (1984) demonstrated that, in fitting the experimental free-ion energy levels of Pr^{3+} (f^2 configuration), the standard deviation could be reduced from 733 cm^{-1} to 24 cm^{-1} by adding nine more parameterized corrective effective operators into the Hamiltonian.

Among several corrective terms included in the effective operator Hamiltonian, a significant contribution to the f^N energy level structure is from configuration interactions between the configurations of the same parity, which can be taken into account by a set of three two-electron operators recommended by Wybourne (1965),

$$\mathscr{H}_{\mathrm{cl}} = \alpha L(L+1) + \beta G(G_2) + \gamma G(R_7), \quad (1.29)$$

where α, β and γ are the parameters associated with $G(G_2)$ and $G(R_7)$ (Rajnak and Wybourne, 1963), the latter being eigenvalues of Casimir operators for the groups G_2 and R_7 (Judd, 1963)

For f^N configurations of $N \geqslant 3$, a three-body interaction term was introduced by Judd (1966) and Crosswhite et al. (1968) as

$$\mathscr{H}_{c2} = \sum_{i=2,3,4,6,7,8} T^i t_i, \tag{1.30}$$

where T^i are parameters associated with three-particle operators t_i. This set of effective operators scaled with respect to the total spin $\boldsymbol{S}$ and total orbital angular momentum $\boldsymbol{L}$ are needed in the Hamiltonian in order to represent the coupling of the f^N states to those in the higher energy configurations (5d, 5p, 5s) via inter-electron Coulomb interactions. It is common to include six three-electron operators $t_i (i = 2, 3, 4, 6, 7, 8)$. When perturbation is carried beyond the second order, an additional eight three-electron operators $t_i (11 \leqslant i \leqslant 19$, with $i = 13$ excluded) are required (Judd and Lo, 1996). A complete table of matrix elements of the 14 three-electron operators for the f-shell were published by Hansen et al. (1996).

In addition to the magnetic spin-orbit interaction parameterized by ζ_{nf}, relativistic effects including spin-spin and spin-other-orbit, both being parameterized by the Marvin integrals M^0, M^2, and M^4 (Marvin, 1947), are included as the third corrective term of the effective operator Hamiltonian (Judd et al., 1968).

$$\mathscr{H}_{c3} = \sum_{i=0,2,4} M^i m_i, \tag{1.31}$$

where m_i is effective operator and M^i is the radial parameter associated with m_i.

As demonstrated by Judd et al. (1968) and Carnall et al. (1983), for improving the parametric fitting of the f-element spectra, two-body effective operators can be introduced to account for configuration interaction through electrostatically correlated magnetic interactions. This effect can be characterized by introducing three more effective operators as

$$\mathscr{H}_{c4} = \sum_{i=2,4,6} P^i p_i, \tag{1.32}$$

where p_i is the operator and P^i is the parameter.

In summary, we have introduced 20 effective operators including those for two- and three-electron interactions. The total effective-operator Hamiltonian of free-ion interactions is

$$\mathscr{H}_{FI} = \sum_{k=0,2,4,6} F^k f_k + \zeta_{nl} A_{SO}(nl) + \alpha L(L+1) + \beta G(G_2) + \gamma G(R_7)$$

$$+ \sum_{i=2,3,4,6,7,8} T^i t_i + \sum_{i=0,2,4} M^i m_i + \sum_{i=2,4,6} P^i p_i. \qquad (1.33)$$

This effective-operator Hamiltonian has been used as the most comprehensive free-ion Hamiltonian in previous spectroscopic analyses of f-element ions in solids (Crosswhite, 1977; Crosswhite and Crosswhite, 1984; Carnall et al., 1984, 1989). The 20 parameters associated with the free-ion operators are adjustable in fitting of experimental data.

1.3.4 Reduced Matrices and Free-ion State Representation

In (1.33), all effective operators for the free-ion interactions have well-defined group-theoretical properties (Judd, 1963a; Wybourne, 1965). Within the intermediate coupling scheme, all matrix elements can be reduced, using the Wigner-Eckart theorem, to new forms that are independent of J, viz.

$$\langle \tau SLJ \mid \mathscr{H}_i \mid \tau' S' L' J' \rangle = P_i \delta_{JJ'} c(SLS'L'J) \langle \tau SL \parallel O_i \parallel \tau' S' L' \rangle, \qquad (1.34)$$

where P_i is the parameter, $c(SLS'L'J)$ is a numerical coefficient, and $\langle \tau SL \parallel O_i \parallel \tau' S' L' \rangle$ is the reduced matrix element of the effective operator O_i. Once the reduced matrix elements are established, it is then not difficult to diagonalize the entire free-ion Hamiltonian with the wave function basis in the *LS*-coupling scheme. All matrix elements of the effective operator Hamiltonian are evaluated in terms of the parameters of the effective operators.

The property of matrix reduction thus allows the matrix of the free-ion Hamiltonian to be reduced into a maximum of 13 independent submatrices for $J = 0, 1, 2, \cdots, 12$ for even N and $J = 1/2, 3/2, 5/2, \cdots, 25/2$ for odd N in an f^N configuration. The numbers of submatrices and their size can be determined from the values of N_J given in Table 1.3. Evaluation of matrix elements is actually a tremendous effort, particularly with inclusion of the effective two- and three-electron operators in the Hamiltonian. For an f^N configuration with $3 < N < 11$, there are more than 10^4 free-ion matrix elements and each of them may have as many as 20 terms to be evaluated on the basis of angular-momentum operations. Fortunately, several groups have made the calculated matrix elements available. For example, one may download from the web site http://chemistry.anl.gov the tables prepared by Crosswhite and co-workers for the free-ion matrix elements, or SPECTRA, to calculate the eigenvalues and eigenfunctions of the free-ion Hamiltonian.

In the Crosswhite files for configurations of f^N with $N = 2$ through 12, the free-ion matrix elements are given in terms of the 20 parameters for all the f^N configurations. As an example, the elements of the free-ion matrix for the $J = 1/2$ submatrix of the f^3 configuration are listed in Table 1.4. Column 3 of Table 1.4 lists the values of the product of $c(SLS'L'J)$ and the values of matrix

elements, Column 4 lists the corresponding parameters. This is one of the simplest cases in which there are only two multiplets: $^4D_{1/2}$ and $^2P_{1/2}$. Except for T^7 and T^8, all 18 other parameters appear in this 2×2 submatrix. Among the interaction terms that contribute to the energy level of these two multiplets, only ζ, $M^{0,2,4}$ and $P^{2,4,6}$ mix the two *LS*-multiplets. In addition, the T^i terms induce a mixture of different multiplets with identical S and L but different τ.

Due to the *SL-S'L'* mixing in the intermediate coupling scheme, labeling a multiplet as $^{2S+1}L_J$ is incomplete. In most cases, the nominal labeling of a free ion state as $^{2S+1}L_J$ only indicates that this multiplet has a leading component from the pure *LS* basis $|LSJ\rangle$. Diagonalization of each of the sub-matrices produces free-ion eigenfunctions in the form (1.15). As an example, for Nd^{3+}, $4f^3$ configuration, we give the leading *LS* terms in the free-ion wavefunctions of the ground states and the excited state at 21,000 cm^{-1}, which were obtained using the values of the parameters listed in Table 1.5:

$$\Psi(4f^3,\ ^4I_{9/2},\ 0\ cm^{-1}) = 0.984\ ^4I - 0.174\ ^2H^1,$$
$$\Psi(4f^3,\ ^2G_{9/2},\ 21,000\ cm^{-1}) = 0.616\ ^2G^1 - 0.494\ ^2G^2 + 0.487\ ^4G + 0.273\ ^4F - 0.208\ ^2H^1,$$

where $^2G^1$ and $^2G^2$ are the first and second $^2G_{9/2}$ terms with $U = (20)$ and (21), respectively, for the *LS* states of f^3 configuration listed in Table 1.3. Other terms with magnitudes less than 0.1 are neglected. These two Nd^{3+} multiplets are commonly labeled as nominal $^4I_{9/2}$ and $^2G_{9/2}$, respectively. In general, *SL-S'L'* mixing becomes more significant in the excited multiplets.

1.3.5 Parameterization of the Free-ion Interactions

One of the characteristics of attempts to parameterize f-configuration spectra is that, because of the heavy mixing of *SL*-basis states brought about by the spin-orbit interactions for each J value, the least-squares fitting method can result in convergence to a false solution. A false solution can be recognized if there is sufficient characterization of the states from supplementary data, such as Zeeman splitting factors or polarized spectra. However, this in itself does not produce the true solution. The true solution can only be found if sufficiently accurate initial parameters are available for the least-squares fitting process to be effective. On the other hand, existing theories of f-element spectroscopy do not accurately reproduce the experimentally observed energy level structure of an f-element ion in solids, and the calculated parameters may be physically different from the phenomenological ones that result from a fitting of the experimental data. Therefore, establishing accurate parameters for the model Hamiltonian essentially relies on systematic analyses that encompass theoretical calculations for incorporating trends of parameter variation across the f-element series. The

Table 1.5 Energy-level parameters for trivalent RE ions in LaF_3 (in cm^{-1}) (Carnall et al., 1989)[a]

	Ce^{3+}	Pr^{3+}	Nd^{3+}	Pm^{3+}	Sm^{3+}	Eu^{3+}	Gd^{3+}	Tb^{3+}	Dy^{3+}	Ho^{3+}	Er^{3+}	Tm^{3+}	Yb^{3+}
F^2		68,878(23)	73,018(19)	76,400	79,805(16)	83,125(31)	85,669(17)	88,995(58)	91,903(69)	94,564(38)	97,483(32)	100,134(23)	
F^4		50,347(69)	52,789(94)	54,900	57,175(45)	[59,268 R]	[60.825 R]	[62,919 R]	64,372(147)	66,397(64)	67,904(67)	69,613(62)	
F^6		32,901(37)	35,757(42)	37,700	40,250(26)	[42,560 R]	44,776(24)	47,252(72)	49,386(139)	52,022(63)	54,010(60)	55,975(104)	
ζ	647(11)	751.7(2)	885.3(1)	1025	1176(1)	1338(3)	1508(2)	1707(2)	1913(2)	2145(1)	2376(2)	2636(1)	2928(10)
α		16.23(0.23)	21.34(0.14)	20.50	20.16(0.89)	[20.16]	18.92(0.83)	18.40(0.19)	18.02(0.23)	17.15(0.11)	17.79(0.20)	17.26(0.30)	
β		−566.6(15)	−593.0(8)	−560	−566.9(8)	[−566.9]	[−600]	−590.9(29)	−633.4(10)	−607.9(6)	−582.1(10)	−624.5(15)	
γ		1371(13)	1445(16)	1475	[1500]	[1500]	[1575]	[1650]	1790(47)	[1800]	[1800]	[1820]	
T^2			298(6)	300	[300]	[300]	[300]	[320]	329(9)	[400]	[400]	[400]	
T^3			35(3)	35	[36]	[40]	[42]	[40]	36(5)	37(2)	43(5)		
T^4			59(4)	58	[56]	[60]	[62]	[50]	127(22)	107(5)	73(5)		
T^6			−285(6)	−310	−347(7)	[−300]	[−295]	−395(28)	−314(16)	−264(16)	−271(11)		
T^7			332(8)	350	373(7)	[370]	[350]	303(17)	404(8)	316(20)	308(18)		
T^8			305(10)	320	348(5)	[320]	[310]	317(13)	315(7)	336(8)	299(17)		
$M^{0(b)}$		2.08(0.3)	2.11(0.1)	2.4	2.60(0.1)	[2.1]	3.22(0.2)	2.39(0.1)	3.39(0.1)	2.54(0.1)	3.86(0.2)	3.81(0.3)	
$P^{2(c)}$		−88.6(47)	192(31)	275	357(28)	[360]	676(75)	373(53)	719(30)	605(24)	594(63)	695(46)	
B_0^2	[−218]	−218(16)	−256(16)	−245	−224(19)	−217(56)	[−231]	−231(24)	−244(18)	[−240]	−238(17)	−249(14)	[−249]
B_0^4	[738]	738(40)	496(73)	470	452(47)	413(86)	[604]	604(49)	506(43)	560(27)	453(90)	457(29)	[457]
B_0^6	[679]	679(48)	641(54)	640	649(47)	558(92)	[280]	280(38)	367(40)	376(28)	373(83)	282(42)	[282]
B_2^2	[−50]	−120(13)	−48(12)	−50	[−50]	[−50]	[−90]	−99(16)	−65(12)	−107(10)	−91(14)	−105(9)	[−105]

continue

	Ce^{3+}	Pr^{3+}	Nd^{3+}	Pm^{3+}	Sm^{3+}	Eu^{3+}	Gd^{3+}	Tb^{3+}	Dy^{3+}	Ho^{3+}	Er^{3+}	Tm^{3+}	Yb^{3+}
B_2^4	[431]	431(27)	521(39)	525	597(29)	[597]	[340]	340(34)	305(33)	250(19)	308(60)	320(21)	[320]
B_4^4	[616]	616(27)	563(41)	490	408(28)	[408]	[452]	452(31)	523(25)	466(19)	417(56)	428(22)	[428]
B_2^6	[-921]	-921(32)	-839(39)	-750	-706(33)	[-706]	[-721]	-721(29)	-590(24)	-576(18)	-489(51)	-482(33)	[-482]
B_4^6	[-348]	-348(41)	-408(35)	-450	-508(34)	[-508]	[-204]	-204(29)	-236(27)	-227(20)	-240(51)	-234(36)	[-234]
B_6^6	[-788]	-788(38)	-831(41)	-760	-692(38)	[-692]	[-509]	-509(33)	-556(25)	-546(22)	-536(49)	-492(36)	[-492]
$\sigma^{(d)}$	7	75	146		232	29	70	146	198	204	127	56	5
$\eta^{(d)}$	51	16	14		13	16	10	12	12	10	19	10	38

(a) Values in parentheses are errors in the indicated parameters. Values in brackets were either not allowed to vary in the parameter fitting, or if followed by an R, were constrained: For Eu^{3+}, $F^4/F^2 = 0.713$, $F^6/F^2 = 0.512$; for Gd^{3+}, $F^4/F^2 = -0.710$; for Tb^{3+}, $F^4/F^2 = 0.707$. All parameters from Pm^{3+} are interpolated values.

(b) M^0 was varied freely, M^2 and M^4 were constrained by the ratios $M^2 = 0.56M^0$, $M^4 = 0.31M^0$.

(c) P^2 was varied freely, P^4 and P^6 were constrained by ratios $P^4 = 0.5P^2$, $P^6 = 0.1P^2$.

(d) Deviation $\sigma = \sum \left[\frac{(\Delta i)^2}{n-p}\right]^{1/2}$, where Δi is the difference between observed and calculated energies, n is the number of levels fit, and p is the number of parameters freely varied.

results of analyses of simpler spectra are carried over to more complex ones through consideration of their symmetry properties (Carnall et al., 1989; Carnall, 1992).

Because lanthanide crystal fields appear as small perturbations on the free-ion levels, efforts to gain a theoretical understanding of free-ion interactions are essential in the development of parametric modeling of crystal field spectra. An important procedure that was taken in establishing the parametric model for f-configurations was to conduct a series of Hartree-Fock (HF) calculations, which, although they require corrections that must be calibrated by comparison with experimental data, predict free-ion parameter trends across the lanthanide series. Detailed results of HF calculations on f-electrons were previously discussed by Crosswhite and Crosswhite (1984) and Carnall et al. (1983).

The most important trends are those of the electrostatic-interaction parameters F^k and spin-orbit parameter ζ_{nf} which increase with the number of f-electrons, N. The experimentally determined values of F^k and ζ_{4f} for trivalent RE ions R^{3+} in LaF_3 and $LaCl_3$ are shown in Fig. 1.2 as a function of N. These values were obtained from systematic analyses of data from a series of experiments (Crosswhite, 1977; Carnall et al., 1989). Figure 1.2 indicates that for trivalent RE ions in crystals, not only the systematic trends are independent of

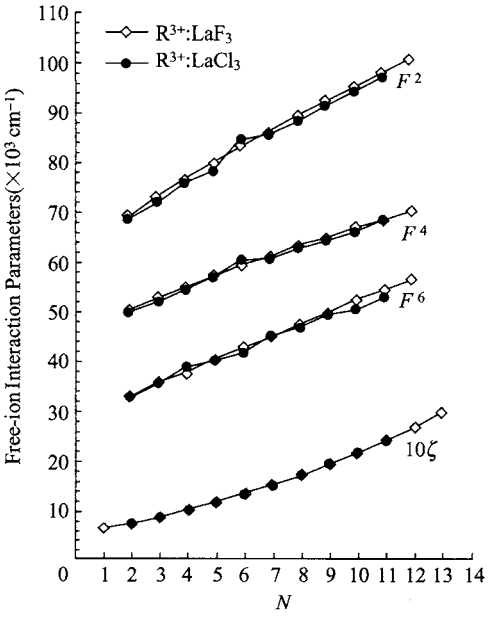

Figure 1. 2 Systematic variation of experimentally determined free-ion interaction parameters F^k and ζ as a function of number of f-electrons (N) for trivalent RE ions R^{3+} in crystal lattice of LaF_3 and $LaCl_3$

hosts, but the values of F^k and ζ_{4f} do not vary significantly in different host crystals. Calculated HF values predict the same trends cross the series, but the HF values of the F^k and ζ_{nf} are always larger than those obtained by allowing them to vary as parameters in fitting experimental data. A comparison is given in Fig. 1.3 between the Hartree-Fock relativistic (HFR) values and experimental values of F^2, F^4, F^6, and ζ_{4f} for trivalent RE ions (Crosswhite, 1977; Carnall et al., 1983). The HFR values of ζ_{4f} agree remarkably with empirical values, while the F^k values remain considerably larger than the empirical values. This is presumably because, in addition to relativistic effects, f-electron coupling with orbitals of higher-lying energies reduces the radial integrals assumed in the HFR approximation. Moreover, the experimental results are frequently obtained for an ion in a condensed phase, not in a gaseous phase, which leads on average to 5% change (Crosswhite, 1977). Because of the absence of mechanisms that absorb these effects in the HFR model, HFR values of F^k cannot be directly used as initial parameters for the least squares fitting process. As shown in Fig. 1.3, although the HFR values of F^k are much larger than the experimental ones, the

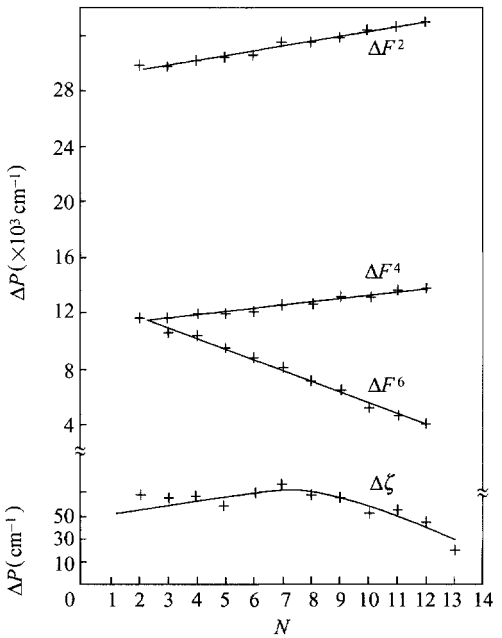

Figure 1.3 Variation of the parameter difference, $\Delta P = P(\text{HFR}) - P(\text{Exp.})$, between the HFR computed values and that determined from experimental data as a function of number of f-electrons

differences between the HFR and the experimental values of F^k have been shown to be nearly a linear function cross the RE series. With this characteristic, linear extrapolations of model parameters from one ion to another lead to values

consistent with those obtained in the actual fitting process.

In addition to HFR calculations of F^k and ζ_{nf}, estimated values for M^k, $k = 0, 2, 4$, can also be computed using the HFR method (Judd et al., 1967). These parameters do not vary dramatically across the f-series. In practice, experience has shown that they can be taken as given or varied as a single parameter by maintaining the HFR ratios $M^2/M^0 = 0.56$ and $M^4/M^0 = 0.31$ (Carnall et al., 1989) (see Table 1.5).

For the rest of the free-ion effective operators introduced above, no direct HF-values can be derived. Only a term-by-term HFR calculation is possible to give additional guidance for parameter estimates. For example, the HFR values of P^ks for Pr^{2+} and Pr^{3+} have been determined by Copland et al. (1971). In establishing systematic trends of parameters for Ln^{3+}: LaF_3, Carnall et al. (1989) constrained the P^k parameters by the ratios $P^4 = 0.5P^2$ and $P^6 = 0.1P^2$ while P^2 was varied freely along with other parameters. These ratios are consistent with the HFR estimation. The variation of these parameters across the series is not significant, and no obvious systematic trends have been established.

Once the systematic trends of free-ion parameters are established, constraints can be imposed on other parameters that are relatively insensitive to the available experimental data. Some parameters such as T^k, M^k and P^k do not vary significantly across the series and to a good approximation have the same values for neighboring ions in the same series. In fact, most of the free-ion parameters are not host sensitive. Typically, there are approximately 1% changes in the values of the free-ion parameters between different lattice environments. Table 1.5 lists parameters for trivalent rare earth ions in LaF_3. The free-ion parameters given in the table can be used as initial inputs for least-squares fitting of energy level structure of a trivalent f-element ion in any crystalline lattice. If there is a limited number of experimental data, one may only allow F^k and ζ_{nf} to vary freely along with the crystal-field parameters and keep other parameters fixed. For further improvement, α, β and γ can be released. For final refinement, M^0 and P^2 may be varied freely with $M^{2,4}$ and $P^{4,6}$ varied following M^0 and P^2 respectively at fixed ratios.

1.3.6 Energy Levels of $4f^N$ Configurations and Binding Energies Relative to Host Band

The free-ion Hamiltonain of Eq. (1.33) and the values of free-ion interaction parameters listed in Table 1.5 are essential in RE spectroscopy and provide a framework useful for analyzing spectra of trivalent RE ions (R^{3+}) in solutions and solids. While the values of free-ion interaction parameters vary within 1% for different hosts, the calculated energy levels of the $4f^N$ multiplets are also expected to vary approximately within 1% for different matrices. The widely-

circulated Dieke chart of energy level structure in the RE series was first created for trivalent ions in $LaCl_3$ based on the analyses of limited spectra (Dieke, 1968) and extended to R^{3+}: LaF_3 by Carnall et al. (1989) with more systematic analyses. The Dieke chart for R^{3+}: LaF_3, Fig. 1.4, is based entirely on the computed energy levels up to 50,000 cm^{-1}, including crystal-field splittings. The computations were conducted with the values of the free-ion and crystal-field parameters listed in Table 1.5. This chart should provide a useful basis for comparison with spectra of trivalent RE ions in other matrices.

While the energy levels of R^{3+} in $4f^N$ configurations extend to higher than 50,000 cm^{-1} for $4 \leqslant N \leqslant 10$, and even extend to higher than 150,000 cm^{-1} for $N=6,7,8$, energy levels accessible by optical excitation are often below 30,000 cm^{-1}. Using excitation with UV sources or two-visible photons, spectra containing energies above 30,000 have been analyzed (Schwiesow and Crosswhite, 1969; Carnall et al., 1989, Liu et al., 1994a) for parameterization of the effective-operator Hamiltonian of Eq. (1.33). Using the values of interaction parameters determined with experimental data for the low-lying states, we anticipate that calculated energy levels below 50,000 cm^{-1} are more accurate than those at higher energies, in which configuration interactions are significant. As a result, the corrections Eqs. (1.35) – (1.38) to the free-ion (and crystal-field, to be discussed in next section) Hamiltonian are either inadequate, or the values of the parameters are expected to be different from these for the low energy states.

So far, we have only discussed the $4f^N$ electronic energy levels of the RE ions. However, interactions between the localized $4f^N$ electronic states of RE ions and the delocalized band states of the crystal lattice can strongly affect the optical properties of technologically important RE-doped materials. Relative energies of $4f^N$ electronic states and crystal band states are important for a fundamental understanding of RE-doped optical materials and a practical understanding of each material's potential performance in specific applications. In contrast to the well-developed understanding of the $4f^N$ states, relatively little is known about the relationships between these states and the electronic states of the crystal. The $4f^N$ ground state binding energies of rare earth ions were recently studied in the gallium garnets by Thiel et al. (2001) using resonant photoemission spectroscopy and compared with the aluminum and iron garnet hosts. The 4d – 4f photoemission resonance was used to separate and identify the $4f^N$ and valence band components of the spectra, and theoretical 4f photoemission spectra were fit to experimental results to accurately determine electron binding energies. A two-parameter empirical model was used to describe the relative energies of the $4f^N$ ground states in these materials. This model can be expressed as

$$E_{4f} = I_{4f} - E_L + \alpha_R(R - R_0) - E_{VBM}, \qquad (1.35)$$

where I_{4f} is the free-ion ionization potential, E_L is the uniform shift experienced

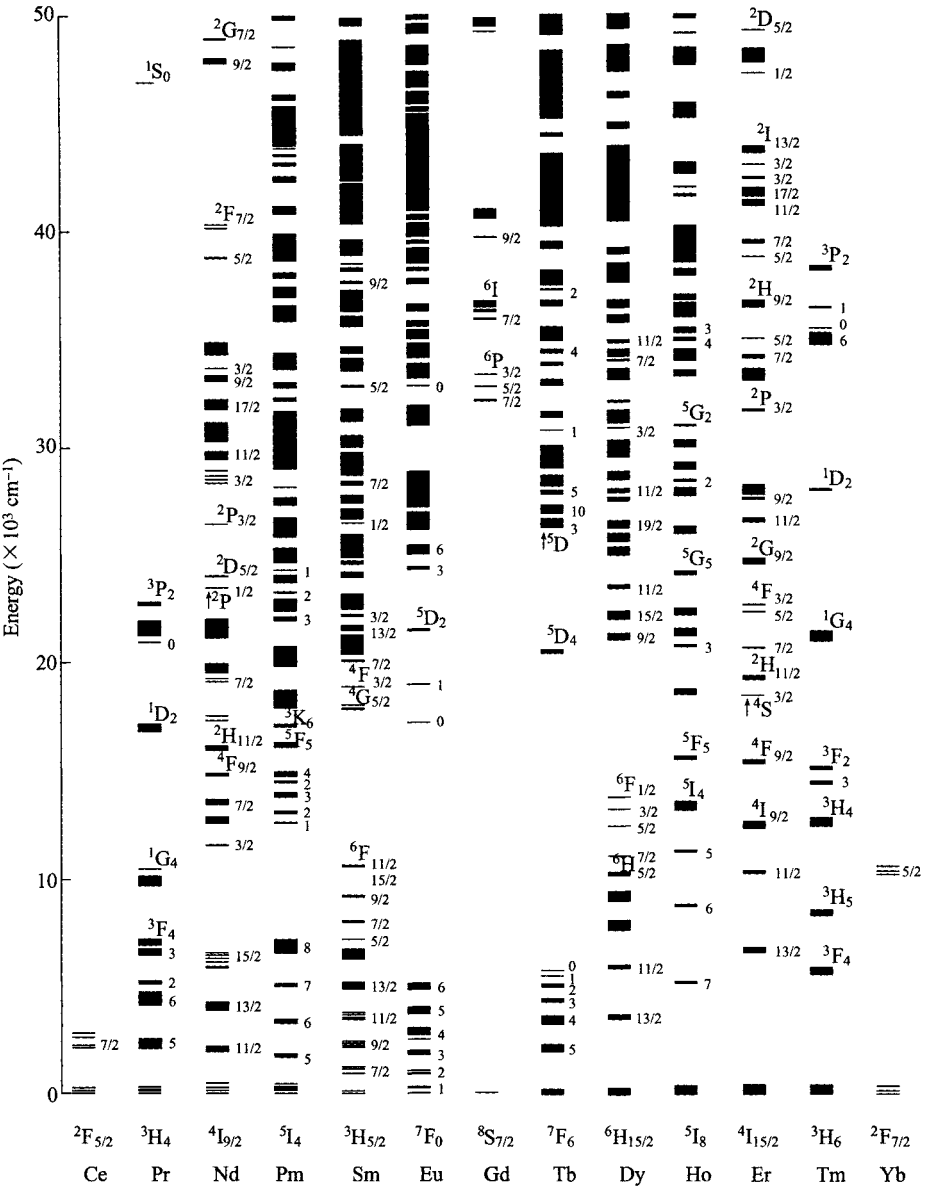

Figure 1.4 Energy level structure of R^{3+}: LaF_3 based on calculated free-ion and crystal-field splittings (Carnall et al., 1989)

by the RE ions, α_R is the binding energy shift per unit change in ionic radius, R and R_0 are the effective ionic radii of the trivalent RE ion and the ionic radius reference. $E_{VBM} = 8.3$ eV is the binding energy of the valence band maximum

(VBM). The value of two parameters in Eq. (1.35), $E_L = 31.6$ eV and $\alpha_R = 9.2$ eV/Å when $R_0 = R(Yb^{3+})$, were obtained by Thiel et al. (2001) in fitting the model to the observed binding energies in gallium garnets. Figure 1.5 shows the calculated and experimental values of binding energies of $4f^N$ electrons in the RE ions relative to VBM in gallium garnets. The experimental data are 7.8, 10.9 and 11.6 eV for TbGG, ErGG, and YbGG, respectively (Thiel et al., 2001), the ionization potentials, I_{4f}, are calculated by Martin et al. (1974), and the effective ionic radii are from Shannon (1976).

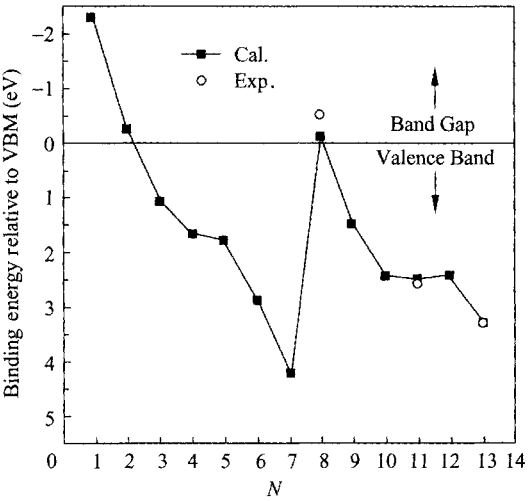

Figure 1.5 Systematic variation of $4f^N$ binding energies relative to the valence band maximum (8.7 eV) in gallium garnets. Circles represent measured binding energies for TbGG (7.8 eV), ErGG (10.9 eV), and TbGG(11.6 eV) (Thiel et al., 2001). The squares connected by solid lines are calculated

The success of this empirical model indicates that measurements on as few as two different RE ions in a host are sufficient to predict the energies of all RE ions in that host. It is shown that systematic shifts in the relative energies of $4f^N$ states and crystal band states between different garnets arise entirely from shifts of the band states, while each RE ion maintains the same absolute binding energy for all garnets studied. These results suggest that further studies of additional host compounds using both photoemission and optical spectroscopy will rapidly lead to a broader picture of the host crystal's effect on 4f electron binding energies.

1.4 Crystal-field Interaction

On placing a rare earth ion in a dielectric crystal, the spherical symmetry of its electronic structure is destroyed, and ionic energy levels split under the influence

of the electric field produced by the crystalline environment. The f-electrons, which participate primarily in ionic bonding with the ligands, have very localized states that are conventionally described in the framework of crystal-field theory (Stevens, 1952; Wybourne, 1965). Using effective operator techniques and the parameterization method, crystal-field theory was developed on the same basis eigenfunctions of the effective operator Hamiltonian for the free-ion interactions as we discussed in the previous section. Applications of group theory along with operator techniques (Tinkham, 1964; Judd, 1963a) have made the crystal-field theory a great success in characterization of the RE ion energy level structure (Görller-Walrand and Binnemans, 1996; Newman and Ng, 2000).

We pointed out in the introduction that, because of the weak ion-ligand interaction, the crystal-field intraconfigurational $4f-4f$ spectra of RE ions contain very sharp spectral lines and are much like the gas phase atomic spectra. The degree to which the $2J+1$ fold degeneracy of a free-ion state is removed depends only on the point symmetry about the ion. The magnitude of crystal-field splittings is determined primarily by the crystal-field strength expressed in terms of the crystal-field parameters of the effective operator Hamiltonian. Because of the complicated electronic interactions in solids, various interaction mechanisms that influence the electronic states of the RE ion in a solid environment may not be accurately calculated in the framework of current crystal-field theory. Evaluation of the crystal-field parameters, however, is theoretically much more difficult than predicting the number of energy levels for each free-ion state. An empirical approach is so far the most effective method for evaluation of the crystal-field parameters (Crosswhite, 1977; Carnall et al., 1984; 1989), while phenomenological modeling and *ab initio* calculations of ion-ligand interactions are able to provide theoretical guidance to the analysis.

From theoretical approaches, analytical expressions of crystal field parameters using phenomenological models are available for calculating the crystal-field parameters of RE ions in specific crystalline lattice. The exchange charge model (ECM) (Malkin et al., 1970, 1987) and the superposition model (SP) (Newman, 1971; Newman and Ng, 1989) are two crystal-field models that have achieved significant success and are very useful for guiding spectrum analysis. From the theoretical point of view, *ab initio* calculations of solid-state electronic energy level structure have advanced significantly along with the rapid development of computer technology and have potential for future applications. However, *ab initio* calculations of f^N crystal field splittings have not reached the accuracy of the observed crystal-field splittings ($< 10\ cm^{-1}$). This accuracy is essential in many cases for determining physical properties of rare earth activated materials (see Chapters 2 – 6).

In this section, we discuss the concepts and methods of crystal field modeling. Applications of empirical methods and model calculations are reviewed with examples of RE activated crystalline materials that have been extensively studied or commonly used as laser media. To gain a more comprehensive understanding of crystal-field theory, the reader may refer to

more detailed reviews (Wybourne, 1965; Hüfner, 1978; Görller-Walrand and Binnemans, 1996; Newman and Ng, 2000).

1.4.1 Crystal-field Hamiltonian and Matrix Element Evaluation

Based on the concept that the crystal-field interaction can be treated approximately as a point charge perturbation on the free-ion energy states, which have their eigenfunctions constructed with the basis of harmonic functions, the effective operators of crystal-field interaction may be defined with the tensor operators of spherical harmonics $\boldsymbol{C}^{(k)}$. Following Wybourne's formalism (Wybourne, 1965), the crystal-field potential may be defined by

$$\mathscr{H}_{\mathrm{CF}} = \sum_{k,q,i} B_q^k C_q^{(k)}(i), \tag{1.36}$$

where the summation involving i is over all the electrons of the ion of interest; B_q^k are crystal-field parameters and, as defined by Eqs. (1.19) and (B.12) in Appendix B, $C_q^{(k)}$ are components of tensor operators $\boldsymbol{C}^{(k)}$ that transform like spherical harmonics.

In addition to Wybourne's formalism for crystal field parameters B_q^k, the older Stevens' notations $A_k^q\langle r^k\rangle$ is often found in the literature. Table 1.6 gives the relationship between B_q^k and $A_k^q\langle r^k\rangle$.

Table 1.6 Relationship between parameters B_q^k and $A_k^q\langle r^k\rangle$

$B_0^2 = 2A_2^0\langle r^2\rangle$	$B_0^6 = 16\,A_6^0\langle r^6\rangle$
$B_2^2 = \frac{\sqrt{6}}{3} A_2^2\langle r^2\rangle$	$B_2^6 = \frac{16\sqrt{105}}{105} A_6^2\langle r^6\rangle$
$B_0^4 = 8A_4^0\langle r^4\rangle$	$B_3^6 = -\frac{8\sqrt{105}}{105} A_6^3\langle r^6\rangle$
$B_2^4 = \frac{2\sqrt{10}}{5} A_4^2\langle r^4\rangle$	$B_4^6 = \frac{8\sqrt{14}}{21} A_6^4\langle r^6\rangle$
$B_3^4 = -\frac{2\sqrt{35}}{35} A_4^3\langle r^4\rangle$	$B_6^6 = \frac{16\sqrt{231}}{231} A_6^6\langle r^6\rangle$
$B_4^4 = \frac{4\sqrt{70}}{35} A_4^4\langle r^4\rangle$	

With the harmonic tensor operators, evaluation of the crystal field matrix elements can be performed with the same methods used for the free-ion matrix elements. With applications of the Wigner-Eckart theorem (Appendix B), the matrix elements of the crystal-field interaction can be expressed with the reduced matrix elements of a unit tensor $\boldsymbol{U}^{(k)}$ (Wybourne, 1965; Weissbluth, 1978):

$$\left\langle l\tau SLJM \left| \sum_i C_q^k(i) \right| l\tau' S'L'J'M' \right\rangle = (-1)^{J-M} \begin{pmatrix} J & k & J' \\ -M & q & M' \end{pmatrix} \times \langle l\tau SLJ \parallel \boldsymbol{U}^{(k)} \parallel l'\tau' S'L'J' \rangle \times \langle l \parallel \boldsymbol{C}^{(k)} \parallel l \rangle. \quad (1.37)$$

In *LS* coupling, the matrix elements of the unit tensor can be further reduced to

$$\langle l\tau LSJ \parallel \boldsymbol{U}^{(k)} \parallel l\tau' L'S'J' \rangle = (-1)^{S+L'+J+k} [(2J+1)(2J'+1)]^{1/2} \times \begin{Bmatrix} J & J' & k \\ L' & L & S \end{Bmatrix} \langle l\tau SL \parallel \boldsymbol{U}^{(k)} \parallel l\tau' L'S' \rangle. \quad (1.38)$$

With Eqs. (1.20), (1.37) and (1.38), we may write the reduced matrix elements of the crystal-field Hamiltonian as

$$\langle l\tau SLJM \mid \mathscr{H}_{\mathrm{CF}} \mid l\tau' S'L'J'M' \rangle = \sum_{k,q} B_q^k (-1)^{J-M} \begin{pmatrix} J & k & J' \\ -M & q & M' \end{pmatrix} D_J^k, \quad (1.39)$$

where

$$D_J^k = (-1)^{S+L'+J+k} [(2J+1)(2J'+1)]^{1/2} \begin{Bmatrix} J & J' & k \\ L' & L & S \end{Bmatrix} \times \langle l\tau SL \parallel \boldsymbol{U}^{(k)} \parallel l\tau' S'L' \rangle (-1)^l (2l+1) \begin{pmatrix} l & k & l \\ 0 & 0 & 0 \end{pmatrix} \quad (1.40)$$

with $l=3$ for f^N configurations. Since all the coefficients, including the values of the 3-j ( ) and 6-j { } symbols, and the doubly reduced matrix elements of the unit tensor, are known for a given free-ion multiplet, it is obvious that evaluation of crystal-field splitting only needs input values of the crystal field parameters B_q^k.

The doubly reduced matrix elements of $\boldsymbol{U}^{(k)}$ may be obtained directly from the tables of Nielson and Koster (1963) or from the SPECTRA program. For configurations of $N > 7$ in the second half of the f-series, the $\boldsymbol{U}^{(k)}$ matrix elements are identical to those of 14-N in the first half of the f-series. The values of the 3-j and 6-j symbols can be obtained from the book of Rotenberg et al. (1959). The values of k and q for which the matrix elements are non-zero are determined by the symmetry of the crystal field and the f-electron angular momentum. For f^N configurations ($l=3$), the 3-j symbols in Eq. (1.40) require that $k=0$, 2, 4, 6, and $|q| \leqslant k$. The values of q are also restricted by the point group of the RE ion site, since the crystal field Hamiltonian has to be invariant under all symmetric operations of the point group. Restrictions due to point group symmetry properties on the non-zero matrix elements of crystal field Hamiltonian

are illustrated in the second part of this section.

For the matrix element of $k = q = 0$, the zero-order of crystal-field interaction is spherically symmetric and does not split the free-ion energy levels, but induces a shift to all energy levels in the same f^N configuration. In general, B_0^0 is not included in evaluation of the crystal-field splitting. Therefore, its contribution to energy level shift is combined with the spherically symmetric component of the free-ion electrostatic interaction. One parameter, namely F^0, absorbs contributions from spherically symmetric components of free-ion and crystal-field interactions.

Once the matrix elements [see Eq. (1.40)] are evaluated, the Hamiltonian of the crystal-field interaction may be diagonalized together with the free-ion Hamiltonian to obtain the crystal-field splitting as a function of the crystal-field parameters. In general, the free-ion parameters may also be considered as variables for fitting an experimental spectrum. As a result, each of the $^{2S+1}L_J$ multiplets splits into crystal-field levels. Because the off-diagonal matrix elements between different J-multiplets may not be zero, as shown in Eqs. (1.39) and (1.40), crystal-field operators can induce J-mixing. Therefore, for RE ions in crystals, both J and M are no longer good quantum numbers.

As a result of J-mixing, as shown in Eq. (B.4) in Appendix B, the eigenfunction of a crystal-field level is of the form,

$$|\mu\rangle = \sum_{J,M} a_{JM} |JM\rangle, \tag{1.41}$$

where, in principle, the summation is over all JM terms of a given f^N configuration. However, inclusion of all J multiplets results in extremely large matrices, particularly, for the configurations with $4 \leqslant N \leqslant 10$. Diagonalization of the effective operator Hamiltonian on the entire $LSJM$ basis could be very time consuming and not actually necessary in an analysis of an experimental spectrum, which usually covers energy levels less than 40,000 cm^{-1}. Off-diagonal matrix elements between free-ion states separated in such a large energy gap are negligibly small. As an approximation, crystal field calculation without including J mixing is appropriate for the isolated multiplets, such as $^1D_2$ of Pr^{3+}, $^8S_{7/2}$ of Gd^{3+}, and $^5D_4$ of Tb^{3+}. In practice, the crystal-field energy level structure of an f^N configuration is usually calculated in a limited energy region in which experimental data are available. Free-ion multiplets with energy levels far from this region may not be included in the calculation. Namely, the eigenfunction basis may be truncated before diagonalizing the matrix of crystal-field Hamiltonian. Theoretically, this truncation of free ion states is legitimate because crystal-field coupling diminishes between two free-ion multiplets as their energy gap increases. From the perturbation point of view, the leading contribution of J mixing to the energy level splitting of the J multiplets is proportional to $1/\Delta E_{JJ'}$. Given that the crystal-field splitting of a free-ion multiplet is on the order of $100 - 1000$ cm^{-1}, the multiplets that are separated by 10^4 cm^{-1} should have no

significant influence on each other.

In computational analyses of experimental spectra, one may truncate the free-ion states whose energy levels are far from the region of interest. This can be readily accomplished after diagonalization of the free-ion matrix to produce the free-ion energy level structure. The later may be considered approximate centers of gravity for the crystal field splitting (Carnall et al., 1984). One chooses the numbers of J multiplets to be included in the crystal-field matrices for each J value. Therefore, the remaining J multiplets are still complete sets of free-ion eigenfunctions that contain all SL components of the given J. This way of free-ion state truncation ensures that no contribution from the free-ion interactions is lost from constructing the free-ion wavefunctions for each J multiplet.

One example is the $^8\mathbf{S}_{7/2}$ ground state of ions in a $4f^7$ configuration for Eu^{2+} and Gd^{3+}, in which both diagonal and off-diagonal matrix elements of crystal field operators vanish. The observed crystal field splittings must be attributed to the contributions of the mixture of other LS terms into the ground state free-ion wavefunction and non-zero off-diagonal matrix elements between different J. Because of large energy gaps from the ground state to the excited multiplets, J mixing is negligible in this case. It has been shown (Liu et al., 1993) that for the $^8\mathbf{S}_{7/2}$ ground state splitting, the leading contributions are from the fourth and higher orders of the coupled matrix elements between the spin-orbit ($\boldsymbol{V}^{(11)}$) and crystal field ($\boldsymbol{U}^{(k)}$) operators. Without inclusion of J mixing, the leading contributions to the crystal-field splitting of the $^8S_{7/2}$ multiplet of an f^7 configuration are from the mixed matrix elements such as

$$\langle {}^8S \| \boldsymbol{V}^{(11)} \| {}^6P \rangle \langle {}^6P \| \boldsymbol{U}^{(2)} \| {}^6D \rangle \langle {}^6D \| \boldsymbol{U}^{(2)} \| {}^6P \rangle \langle {}^6P \| \boldsymbol{V}^{(11)} \| {}^8S \rangle$$

and

$$\langle {}^8S \| \boldsymbol{V}^{(11)} \| {}^6P \rangle \langle {}^6P \| \boldsymbol{U}^{(6)} \| {}^6I \rangle \langle {}^6I \| \boldsymbol{U}^{(6)} \| {}^6P \rangle \langle {}^6P \| \boldsymbol{V}^{(11)} \| {}^8S \rangle.$$

It is obvious that truncation of LS terms in the $J = 7/2$ multiplets should affect the scale of the coupled matrix elements, and thus affect the crystal-field splitting. The same effect is expected for the off-diagonal matrix elements between different J, but this is less important because of the large energy gap between the ground state and the first excited state.

In the literature, the crystal-field interaction is often characterized by quantitative comparison of the crystal-field strength defined as (Auzel, 1983)

$$N_v = \left[\frac{1}{4\pi} \sum_{q,k} \frac{(B_q^k)^2}{2k+1} \right]^{1/2}, \tag{1.42}$$

or as (Chang et al., 1982)

$$S = \left\{ \frac{1}{3} \sum_{k=2,4,6} (2k+1)^{-1} \left[(B_0^k)^2 + 2 \sum_{q>0} | B_q^k |^2 \right] \right\}^{1/2}. \qquad (1.43)$$

1.4.2 Symmetry Rules

We now discuss the geometric properties of the crystal-field operators and parameters in more detail. In addition to the angular momentum of the RE ions that restricts k and q for a set of non-vanishing crystal-field operators, the site symmetry of RE ion in a crystalline lattice also imposes limits on crystal field operators, because the tensor operators for the crystal-field interaction must be invariant under the point group symmetry operations. Here our interest is to identify the non-vanishing components of crystal-field operators and their matrix elements. First, if we restrict our attention to the states of the same parity, namely $l = l'$, k must have even values. It is also required that B_q^k must be real in any symmetry group that contains a rotation operation about the Y-axis by π or a reflection through the X-Z plane; otherwise $B_q^k (q \neq 0)$ is complex. In the later case, one of the B_q^k can be made real by a rotation of system of coordinates about the Z-axis. The B_q^k for $q < 0$ are related to the imaginary ones for $q > 0$ by

$$B_{-q}^k = (-1)^q B_q^{k*}. \qquad (1.44)$$

Also under the invariant conditions of the point group theory, the crystallographic axis of lowest symmetry determines the values of q for the non-vanishing crystal-field operators. For example, at a site with C_{3v} symmetry, there is a threefold axis of rotational symmetry with a reflection plane that contains the C_3 axis (Tinkham, 1964; Hüfner, 1978). The ligand electric field must exhibit this symmetry and hence if a $2\pi/3$ rotation is made on the crystal field potential, followed by a reflection with regard to the plane, the potential is invariant only if $q = 0, \pm 3$, and ± 6. Thus, within an f^N configuration, the crystal field Hamiltonian may be written as

$$\begin{aligned} \mathcal{H}(C_{3v}) = \sum_i \{ & B_0^2 C_0^{(2)}(i) + B_0^4 C_0^{(4)}(i) + B_3^4 [C_{-3}^{(4)}(i) - C_3^{(4)}(i)] \\ & + B_0^6 C_0^{(6)}(i) + B_3^6 [C_{-3}^{(6)}(i) - C_3^{(6)}(i)] \\ & + B_6^6 [C_{-6}^{(6)}(i) + C_6^{(6)}(i)] \}. \end{aligned} \qquad (1.45)$$

If the reflection plane is perpendicular to the C_3 axis, the site symmetry becomes C_{3h}, which occurs for RE ions in all the lanthanide ethylsulfates and trichlorides such as $LaCl_3$ and bromides such as $LaBr_3$ (Morosin, 1968). The potential invariant property requires $q = 0, \pm 6$ only, but since there is no rotation symmetry about the y-axis by π or a reflection through the X-Z plane for the C_{3h}

site, there is an imaginary non-cylindrical term in the Hamiltonian:

$$\mathscr{H}(C_{3h}) = \sum_j \{B_0^2 C_0^{(2)}(j) + B_0^4 C_0^{(4)}(j) + B_0^6 C_0^{(6)}(j) + B_6^6[C_{-6}^{(6)}(j) + C_6^{(6)}(j)] + iB'^6_6[C_6^{(6)}(j) - C_{-6}^{(6)}(j)]\}. \tag{1.46}$$

D_{3h} is a symmetry group that includes all rotation and reflection operations of C_{3v} and C_{3h}(Tinkham, 1964; Hüfner, 1978). The crystal field operators for RE ions at a D_{3h} site are the real terms for C_{3h} without the imaginary term $iB'^6_6(C_6^{(6)} - C_{-6}^{(6)})$. The non-vanishing terms of crystal field operators for various lattice sites of RE ions in crystals are listed in Table 1.7.

Table 1.7 Non-vanishing terms of crystal-field (CF) parameters B_q^k, numbers of reduced matrices and crystal-field quantum number μ for f^N configurations in crystals of various symmetries[a, b]

Crystal structure	Site symmetry	Example	B_q^k	μ (S, D, T, Q)[c] for even N	μ (S, D, T, Q)[c] for odd N
Monoclinic	C_s, C_2, C_{2h}	LaF_3	B_0^2, B_0^4, B_0^6, Re(B_2^2) $B_2^4, B_2^6, B_4^4, B_4^6, B_6^6$	S: ±0, ±1	D: 1/2
Rhombic	C_{2v}, D_2, D_{2h}	$Y_3Al_5O_{12}$	B_0^2, B_0^4, B_0^6, Re(B_2^2, $B_2^4, B_2^6, B_4^4, B_4^6, B_6^6$)		
Trigonal	C_3, $S_6(C_{3i})$	$LiNbO_3$	B_0^2, B_0^4, B_0^6, Re(B_3^4), B_3^6, B_6^6	S: ±0 D: 1	D: 1/2, 3/2
	C_{3v}, D_3, D_{3d}	Y_2O_2S	B_0^2, B_0^4, B_0^6, Re(B_3^4, B_3^6, B_6^6)		
Tetragonal	C_4, S_4, C_{4h}	$LiYF_4$	B_0^2, B_0^4, B_0^6, Re(B_4^4), B_4^6	S: ±0, ±2, D: 1	D: 1/2, 3/2
	D_4, C_{4v}, D_{2d}, D_{4h}	YPO_4	B_0^2, B_0^4, B_0^6, Re(B_4^4, B_4^6)		
Hexagonal	C_6, C_{3h}, C_{6h}, D_6, C_{6v}, D_{3h}, D_{6h}	$LaCl_3$	B_0^2, B_0^4, B_0^6, Re(B_6^6)	S: ±0, ±3 D: 1, 2	D: 1/2, 3/2, 5/2
Cubic	T, T_d, T_h, O, O_h	CeO_2	B_0^4, B_0^6, Re(B_4^4, B_4^6)[d]	S: ±0, ±4 D: 2, 6 T: 1	D: μ = 1/2, 7/2 Q: μ = 3/2

(a) Morrison et al., 1982;
(b) Hüfner, 1978;
(c) S: singlet, D: doublet, T: triplet, Q: quadruplet;
(d) $B_4^4 = \frac{5}{\sqrt{70}} B_0^4$, $B_4^6 = -\sqrt{\frac{7}{2}} B_0^6$.

Because of the 3-j symbols in Eq. (1.39), the degeneracy in M may be completely or partially removed by crystal-field coupling between states of different JM. In the crystal-field matrix, the terms for which $M - M' = q$ are mixed by $C_q^{(k)}$. Otherwise the crystal-field matrix elements are zero. Based on this property, the crystal-field matrix may be reduced into a number of independent submatrices each of which is characterized by a crystal quantum number μ (or Γ). Each μ represents a group of M, such that $M - M' = q$ (0, 2, 3, 4, 6) belongs to the same submatrix (Hüfner, 1978). All matrix elements between the submatrices are zero. The crystal-field quantum number may be used to classify the crystal-field energy levels even when J and M are not good quantum numbers. To consider C_{3h} (and D_{3h}) as an example, the JM and $J'M'$ with $M - M' = 6$ belong to the same crystal-field submatrix. For even number of f electrons, there are four independent submatrices, and for odd number of f electrons, there are three independent submatrices. The parameters of non-vanishing crystal-field terms for symmetries of common crystal hosts of f-element ions are given in Table 1.7 along with the numbers of reduced crystal-field matrices.

Without a magnetic field, the electrostatic crystal field alone does not completely remove the free-ion degeneracy for the odd-numbered electronic configurations. Known as Kramers' degeneracy (Kramers, 1930), all crystal field levels are at least doubly degenerate. The crystal quantum number and JM classification are given for C_{3h} and D_{3h} in Table 1.8. In calculation of energy level structure for degenerate doublets, one may cut off a half of the submatrix elements.

In many cases, calculations of crystal-field energy levels have been successful by using higher site symmetry than the real one so that a smaller number of parameters are required. First of all, this is because RE ions in many solids occupy a low site symmetry and the limited number of observed energy levels could not accurately determine a large number of crystal-field parameters. Secondly, many crystal lattices do not have mirror symmetries in their coordinates so that the crystal-field parameters with $q \neq 0$ are complex (see Table 1.7). If one makes an approximation by using only the real part of the crystal-field operators, the energy level calculation becomes much easier. Since the high symmetry approximation is equivalent to up-grading a lower symmetry site to a higher one within the same symmetry group, this is called the descent-of-symmetry method (Görller-Walrand and Binnemans, 1996). This method may be applied to the groups of monoclinic, trigonal, and tetragonal structures listed in Table 1.7. For example, the S_4 site symmetry of trivalent lanthanide ions in $LiYF_4$ is often treated as D_{2d} (Esterowitz, 1979; Görller-Walrand, 1985, Liu et al., 1994a). Similarly, the actual C_2 symmetry of LaF_3 is replaced by C_{2v} (Carnall et al., 1989) and the C_{3h} symmetry of $LaCl_3$ by D_{3h} (Morrison and Leavitt, 1982).

Table 1.8 Classification of crystal field energy levels for C_{3h} and D_{3h} symmetry

(a) Even number of electrons

J	$M(\mu=0$ $^1\Gamma_{12})$	$M(\mu=\pm1$ $^2\Gamma_5)$	$M(\mu=\pm2$ $^2\Gamma_6)$	$M(\mu=3$ $^1\Gamma_{34})$	No. (Levels)
0	0				1
1	0	±1			2
2	0	±1	±2		3
3	0	±1	±2	3, −3	5
4	0	±1	±2, ∓4	3, −3	6
5	0	±1, ∓5	±2, ∓4	3, −3	7
6	−6, 0, 6	±1, ∓5	±2, ∓4	3, −3	9
7	−6, 0, 6	±7, ±1, ∓5	±2, ∓4	3, −3	10
8	−6, 0, 6	±7, ±1, ∓5	±8, ±2, ∓4	3, −3	11

(b) Odd number of electrons

J	$M(\mu=\pm12$ $^2\Gamma_7)$	$M(\mu=\pm3/2$ $^2\Gamma_8)$	$M(\mu=\pm5/2$ $^2\Gamma_9)$	No. (Levels)
1/2	±1/2			1
3/2	±1/2	±3/2		2
5/2	±1/2	±3/2	±5/2	3
7/2	±1/2	±3/2	±5/2, ∓7/2	5
9/2	±1/2	±3/2, ∓9/2	±5/2, ∓7/2	6
11/2	±1/2, ∓11/2	±3/2, ∓9/2	±5/2, ∓7/2	7
13/2	±13/2, ±1/2, ∓11/2	±3/2, ∓9/2	±5/2, ∓7/2	8
15/2	±13/2, ±1/2, ∓11/2	±15/2, ±3/2, ∓9/2	±5/2, ∓7/2	9

In practical cases, the crystal field of C_{3h} symmetry has been found to exhibit an effective potential appropriate to D_{3h} symmetry because the imaginary term of $\mathrm{Im}B_6^6$ in the C_{3h} potential is negligibly small. This is known because the nearest ligands have D_{3h} symmetry. When the second shell of coordination is considered, the site symmetry reduces to C_{3h} because the second nearest ligands add a smaller contribution to the crystal field at the lanthanide site. As illustrated in Fig. 1.6 on the X-Y plane, a rotation ($\Delta\phi$) of the next nearest ligand (NNL) coordinates about the Z-axis converts the structure of $LaCl_3$ from C_{3h} to D_{3h} symmetry. For the actual structure of the lanthanide ethylsulfates and trichlorides, $\Delta\phi$ may be less than 1°. Similarly for lanthanide ions in $LiYF_4$, the value of $\mathrm{Im}B_4^6$ in the S_4 potential is less determined. With zero $\mathrm{Im}B_4^6$, an effective site symmetry of D_{2d} has been used in practical cases (Morrison and Leavitt, 1982).

Conversion of the $LiYF_4$ structure from S_4 symmetry to D_{2d} symmetry only involves the NNL fluorine ions connected in a tetrahedron. The actual crystallographic site symmetry is a slight distortion of D_{2d}. This implies a distortion of the ϕ-coordinates from the dodecahedron D_{2d} values (Blanchfield, 1983; Urland, 1981). In addition to a rotation of $\Delta\phi$ about the Z-axis, a small change in the radial distance from the Y^{3+} center to the NNL is required in order to construct a perfect D_{2d} symmetry for the two tetrahedrons of the fluorine ions.

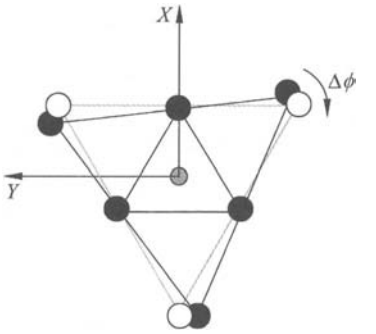

Figure 1. 6 Illustration of descent-of-symmetry operations for $LaCl_3$ type of hexagonal crystals. A rotation of the next nearest lignds on the larger trigonal prism by a small angle $\Delta\phi$ about the Z-axis converts C_{3h} to D_{3h}. The next nearest ligands move from their actual positions to the D_{3h} sites shown by the circles

In general, use of the descent-of-symmetry method may have more complicated consequences than that of the above two examples. For a specific symmetry modification, one may estimate the changes in crystal-field parameters based on the rotation symmetry of point charges in polar coordinates (θ, ϕ) and assume that ligand ions in each shell of coordination are at the same distance from the f-element ion. For an arbitrary rotation, the B_0^k parameters should only depend on the θ-coordinates, whereas the B_q^k parameters ($q \neq 0$) depend on both θ- and ϕ-coordinates. Changes in the ϕ-coordinates have no influence on B_0^k and $|B_q^k| = [(\mathrm{Re}B_q^k)^2 + (\mathrm{Im}B_q^k)^2]^{1/2}$. Descent-of-symmetry operations that have this property are $C_{nh} \rightarrow D_{nh}$, $S_4 \rightarrow D_{2d}$, and $C_n \rightarrow C_{nv}$. The symmetry changes that incorporate a change in θ-coordinates will change all parameters, such as $D_{nh} \rightarrow C_{nv}$ and $D_{nh} \rightarrow C_n$. If the symmetry of the f-element site is lowered, not only are additional parameters required, but there are also changes in the crystal-field parameters present in the higher symmetry. Therefore, there is far less rational for using D_{nh} as an approximation for C_n and C_{nv}.

As mentioned above, site distortion is a common phenomenon when doping f-element ions into crystals. A dopant ion likely has a lower symmetry site than that of the host ion. Accordingly, both the sign and magnitude of crystal-field parameters are subjected to change. The descent-of-symmetry, although not

realized, is actually enacted in analyses of the crystal-field spectra of doped systems in which lowering the site symmetry does not necessarily further reduce the degeneracy of the energy states. As we discussed above, different crystal structures may undergo different types of distortion that reflect the properties of the specific coordination polyhedra in a given crystal. Görller-Walrand and Binnemans (1996) gave a detailed description of the effects of structure distortion in terms of changes in the θ- and ϕ-coordinates. However, changes in radial distances may occur as well. For ions at a distorted site that further reduces the degeneracy of electronic states, analyses of crystal-field spectra must be conducted using a lower symmetry, although in many cases determination of actual site symmetry is difficult. An extensively studied system is trivalent rare earth ions in CaF_2 which has an intrinsic site of cubic symmetry. Due to charge imbalance between a trivalent dopant and a Ca^{2+} ion, more than 20 distinct defect sites have been identified (Seelbinder and Wright, 1979; Tissue and Wright, 1987). In addition to cubic site symmetry, defect sites of C_{4v}, C_{3v} were also found, and many of these defect sites have symmetries lower than C_{nv}.

1.4.3 Empirical Evaluation of Crystal-field Parameters

In modeling crystal-field splittings, we have the same problems as we pointed out in Section 1.3.5 for parameterization of the free-ion Hamiltonian. Theoretical calculations do not accurately reproduce the observed spectra, while the least-squares method for empirical evaluation of crystal-field parameters can result in convergence to a false solution. However, from the experimental point of view, theoretical calculations using the point charge approximation provide a necessary guidance to establishing the parameters for the effective operator Hamiltonian. For RE ions in crystals of well-defined site symmetry, crystal-field theory is widely used along with group theory for predicting the number of energy levels and determining selection rules for electronic transitions between crystal-field levels (see Chapter 2). Whereas the number of non-vanishing crystal-field parameters can be determined by the symmetry arguments, their values are usually determined by analyzing the experimentally observed crystal-field splittings. In general, abundant experimental data that carry supplementary spectroscopic information, such as polarized transitions allowed by electric or magnetic dipolar coupling, ensure the accuracy of the experimentally fitted crystal-field parameters (Liu et al., 1994a). In addition, temperature dependence of crystal-field splitting may be analyzed to distinguish pure electronic lines from vibronic features (see Chapter 3). If multiple sites exist, site-resolved spectra are required to distinguish energy levels of ions at different sites (Tissue and Wright, 1987; Liu et al., 1994a, b). Accordingly, as a procedure of parametric modeling, correct assignment of observed energy levels to the calculated ones is crucial to avoid a false solution. For spectra that lack sufficient experimental information for exclusive assignment, this procedure may

involve several iterations of trial calculations and analyses that again require understanding the basics of crystal-field splitting of free-ion states (Carnall et al., 1989; Carnall, 1992). Based upon the symmetry properties expressed as 3-j symbols in Eqs. (1.39) and (1.40), several criteria may be applied with the assumption that J mixing is small, which is true for isolated multiplets:

(1) Splitting of $J=1$ (or 3/2) states depends only on B_q^2; that of $J=2$ (or 5/2) depends on B_q^2 and also on B_q^4;

(2) The B_0^k parameters dominate splittings between the crystal-field levels that have the same leading M components;

(3) The sign of crystal-field parameters determines the ordering of crystal-field levels in terms of $\mu(JM)$.

For setting initial parameters of the crystal-field Hamiltonian to be fitted by observed energy levels, one may simply use the previously established parameters for different f-element ions in the same or similar host materials. For the entire series of trivalent rare earth ions in one of the most extensively studied crystals LaF_3, the parameters of free-ion and crystal-field interactions are listed in Table 1.5. Comprehensive summaries of previously studied systems were given by Morrison and Leavitt (1982) and also by Görller-Walrand and Binnemans (1996). Alternatively, the signs and magnitudes of crystal-field parameters can be predicted according to the coordination of the f-element ion and using the point charge model of electrostatic crystal-field potential. For this purpose, only the nearest ligand (NL) atoms need to be considered. As a function of the radial and angular coordinates, the expressions for the B_q^k parameters are given in next section. The signs of the crystal-field parameters are merely determined by the angular part of the electrostatic potential and may be obtained by symmetry analysis. The predicted signs are of great importance for checking the signs of the parameters obtained by the fitting procedure. Some sign combinations may correspond to a coordination that is physically impossible. Generally, determination of the magnitudes requires more quantitative calculations of the overlap integrals between the f-electrons and the electrons of the ligands. The electrostatic interactions beyond the nearest ligands may bring about significant contributions to the parameters with $k = 2$. For those parameters, the total contribution from the long range interactions may exceed that of the NL so that a change in the sign of B_q^2 determined by the NL atoms is possible (Zhorin and Liu, 1998). Moreover, the electrostatic point charge model is not realistic in describing the short-range interactions between the f-element ion and its nearest ligands. Charge exchange interactions including covalent effect may dominate the crystal-field parameters with $k=4, 6$. For these reasons, the empirical approach with theoretical guidance is necessary to ensure that the parameterization is within the limitations of physical interactions.

In a nonlinear least-squares fitting process, the magnitudes and signs of crystal-field parameters are varied to best reproduce the observed energy level structure. This is actually a process of optimizing crystalline structure within a

given restriction through variation of the crystal-field parameters. The parameters that have higher weight are better determined than the parameters that have less influence on the observed energy levels. Adding an imaginary parameter may only change the real part of the term that has the same q and k but does not have much influence on other parameters. If the values of the crystal-field parameters for a system of higher symmetry are used as initial values of the parameters for a different system of lower symmetry, the fitting may either fall into a false solution or leave the added parameters less determined. In this case, one should assign the unambiguously observed energy levels, most likely the isolated multiplets, and only allow the most weighted crystal-field parameters to vary freely. Once these weighted parameters settled down, further fitting should be performed on the entire set of crystal-field parameters along with the variation of the free-ion parameters.

1.4.4 Theoretical Evaluation of Crystal-field Parameters

Quantum mechanical calculations of crystal-field energies and corresponding crystal-field parameters for RE ions in compounds with different chemical characteristics were carried out by several groups of authors in the framework of the cluster approximation. For a RE ion and its nearest ligands (chlorine, fluorine or oxygen ions), the fully antisymmetric and orthonormalized wave functions of zero-order are constructed as linear combinations of products of individual ion wave functions, and the energy matrix is built with the complete Hamiltonian that contains one- and two-electron operators including the interaction with the electrostatic field created by the rest of the crystal. The effective crystal-field Hamiltonian is introduced satisfying the requirements that its matrix elements in the basis of 4f-functions of the RE ion coincide with the corresponding matrix elements of the complete Hamiltonian (see Appendix A). The first order contributions to the energy matrix include integrals over one-electron wave-functions of the occupied states of the cluster. Higher order contributions correspond to configuration mixing. The procedure and details of calculations have been described in original and review papers by Newman (1971), Eremin (1989), Garcia and Faucher (1995), Shen and Bray (1998), and Newman and Ng (2000). Here we present only a brief description of the results of *ab initio* simulations that are important for modeling of the main physical mechanisms responsible for crystal-field splittings in the spectra of RE ions.

The first order terms in the energy matrix include Coulombic, exchange and overlap integrals over 4f orbitals of the RE ion and outer orbitals of ligand ions. From these terms, the 4f-electron energy in the electrostatic field of the ligand point multipole moments and the charge penetration contribution may be singled out. The second order terms may be classified according to the intermediate (virtual) excited state of the cluster. In this regard, the following electronic

excitations are considered:

(1) Intra-ion excitations from the filled electronic shell of the RE ion to the empty excited shell (in particular, $5p^6 \rightarrow 5p^5 5d^1$). These processes shield the inner valence $4f^N$-shell and may be accounted for, at least partly, by introducing shielding (or antishielding) factors into the multipole moments of the valence electron ($\langle 4f|r^k|4f\rangle \rightarrow (1-\sigma_k)\langle 4f|r^k|4f\rangle$) (Rajnak and Wybourne, 1964). The shielding factors for RE ions were computed by Gupta and Sen (1973) using the variational method.

(2) Intra-ion excitations from the valence shell into empty shells and from the filled shells into the valence shell (in particular, $4f^N \rightarrow 4f^{N-1}5d^1$ or $5p^6 \rightarrow 5p^5 4f^{N+1}$). These processes contribute to the linear shielding and cause additional corrections to parameters of the effective Hamiltonian bilinear in parameters of the electrostatic field.

(3) Inter ion excitations, mainly into the charge transfer states of the RE ion with the extra electron in the valence shell excited from the ligand outer filled shell. Actually, mixing of the ground configuration with the charge transfer states corresponds to the partial covalent character of chemical bonding between an RE ion and its ligands.

It should be noted that the effective Hamiltonian (see Eq. (1.36)) with a single set of crystal-field parameters, operating within the total space of wave functions of the $4f^N$ configuration, can be introduced if all excited configurations of the cluster under consideration are separated from the ground configuration by an energy gap that is much larger than the width of the energy spectrum of the ground configuration. Otherwise the crystal-field parameters become term (*LSJ*) dependent. In particular, the crystal-field analysis fulfilled on an extended basis containing the ground $4f^2$ and excited 4f5d, 4f6p configurations of Pr^{3+} in YPO_4 (Moune et al., 2002) greatly improved the agreement between the experimental data and the calculated energy levels. An example of the quasiresonant mixing of the ground $4f^{13}$ configuration with the charge transfer states of the $Yb^{3+}Br_6^-$ cluster in $CsCdBr_3$ and its effect on the splitting of the excited $^2F_{5/2}$ multiplet of the Yb^{3+} ion was described by Malkin et al. (2000).

A general conclusion concerning the dominant role of overlap and covalent contributions to the crystal-field parameters B_q^4 and B_q^6 follows from all *ab initio* calculations carried out up to the present time. When the Hartree-Fock one-electron wave functions of free ions are used in simulations, relative differences between the theoretical and experimental values of these parameters do not exceed 50%. However, for the parameters B_q^2 of the quadrupole component of the crystal field, contributions from the long-range interactions of valence electrons with point charges, dipole and quadrupole moments of ions in the crystal lattice are comparable to contributions from the interactions with the nearest ligand ions, and the theoretical estimations differ substantially from the experimental data.

Whereas the free-ion parameters vary smoothly across the 4f series, series